Noise-Induced Schooling of Fish

Jitesh Jhawar,[1,*] Richard G. Morris,[2,3,*] U. R. Amith-Kumar,[1]
M. Danny Raj,[4] Tim Rogers,[5] Harikrishnan R.,[1] and Vishwesha Guttal[1]

[1]*Centre for Ecological Sciences, Indian Institute of Science, Bengaluru, India.*
[2]*School of Physics and EMBL-Australia node in Single Molecule Science, University of New South Wales, Sydney, Australia.*
[3]*Simons Centre for the Study of Living Machines, National Centre for Biological Sciences, TIFR, Bengaluru, India.*
[4]*Department of Chemical Engineering, Indian Institute of Science, Bengaluru, India.*
[5]*Centre for Networks and Collective Behaviour, Department of Mathematical Sciences, University of Bath, Bath, UK.*

We report on the dynamics of collective alignment in groups of the cichlid fish, *Etroplus suratensis*. Focusing on small-to-intermediate sized groups ($10 \lesssim N \lesssim 100$), we demonstrate that schooling (highly polarised and coherent motion) is noise-induced, arising from the intrinsic stochasticity associated with finite numbers of interacting fish. The fewer the fish, the greater the (multiplicative) noise and therefore the likelihood of alignment. Such rare empirical evidence tightly constrains the possible underlying interactions that govern fish alignment, suggesting that *E. suratensis* either spontaneously change their direction or copy the direction of another fish, without any local averaging (the otherwise canonical mechanism of collective alignment). Our study therefore highlights the importance of stochasticity in behavioural inference. Furthermore, rather than simply obscuring otherwise deterministic dynamics, noise can be fundamental to the characterisation of emergent collective behaviours.

Over the past decade, modern methods of image analysis and tracking have been used extensively to study the collective motion of animal groups, and by proxy the social interactions between their constituent individuals. Using a variety of techniques, a broad range of taxa have been investigated so far, including flocks of starlings [1–3], shoals of fish [4–8], marching locusts [9, 10], mice [11] and red deer [12]. However, aside from [13]— a theoretical follow-up to the pioneering study of direction-switching in locust nymphs [10]— such empirical studies have overlooked the *intrinsic noise* that arises in any finite collective, or group, whose underlying individuals interact in an inherently probabilistic way.

We argue that this is a significant oversight; system-size expansions of Master equations [14] readily demonstrate that probabilistic individual behaviours can conspire to produce collective features that are wholly surprising. Such approaches are typically referred to as *mesoscopic*, since they describe the properties of large-but-finite sized groups, where the stochastic behaviour of the individuals cannot be completely 'averaged-out'. Notably, such residual stochasticity often manifests as a multiplicative, or state-dependent noise at the collective level. In many cases, this can give rise to 'finite-size noise-induced' behaviour [15, 16] where the probability of finding the system in a partiular state is concentrated away from the deterministic ($N \to \infty$) fixed point(s). For example, in a toy model of binary choice (between two food sources, say) where individuals can either copy each other at random or spontaneously change their mind, no consensus is ever reached in the $N \to \infty$ limit. By contrast, at finite group sizes, noise-induced effects imply a clear consensus, with the group choosing either one of the options with equally high probability [17].

Such ideas are particularly relevant for the *inference* of individual behaviours from collective-level data. The important point being that, rather than simply obscuring the signature of otherwise deterministic dynamics, collective-level noise can actually encode important information about individual interactions [18]. Therefore, not only should fluctuations be extracted from data with care, but they are also pertinent to a major challenge of modern behavioural inference: how to distinguish between multiple mechanisms that ostensibly reproduce the same qualitative features of collective motion.

It is in this context that we report on the stochastic dynamics of directional alignment in freshwater fish (*Etroplus suratensis*) under controlled laboratory conditions. We use a data-driven approach, formally extracting a stochastic differential equation (SDE) that describes the dynamics of collective alignment. We find that schooling in such fish— *i.e.*, highly polarised and coherent motion— bears all the hallmarks of a finite-size noise-induced effect, resulting from finite sized groups of individuals that interact according to probabilistic rules. Put simply, the smaller the number of fish in a group, the larger the stochastic fluctuations and surprisingly, the greater the ordering. This counter-intuitive result can be traced-back to an $O(1/\sqrt{N})$ noise term that is multiplicative— *i.e.*, where the strength of noise depends on the collective state of the group.

Significantly, the type of finite-size noise-induced schooling that we observe tightly constrains the possible interactions between fish that might underpin it. Using both analysis and computer simulations, we find that all the salient features of our data are captured by a simple stochastic protocol for pairwise interactions, whereby a given fish interacts and aligns with other (single) fish, one at a time. Such features are *not* present if ternary, or higher-order aligning interactions are dominant, including local directional averaging, as used in the Vicsek-like family of approaches [19, 20]— the *de facto* standard for modelling collective motion.

[*] These authors contributed equally to the manuscript.

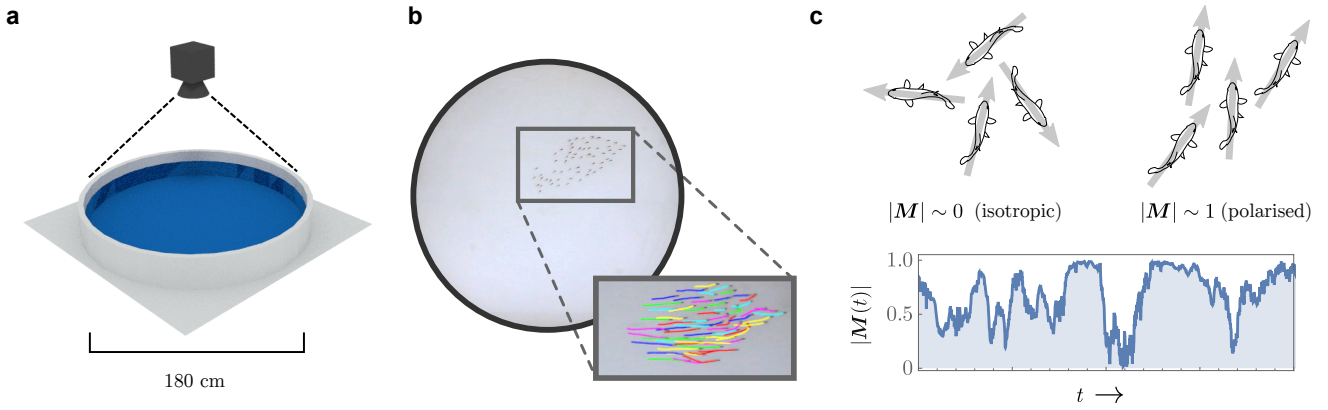

FIG. 1. **Capturing the stochastic dynamics of ordering in small-to-medium sized groups of fish**. Schools of juvenile *Etroplus suratensis* were filmed in a large shallow tank (180 cm diameter, 10 cm height), under controlled laboratory conditions (panel **a**). Using particle tracking methods, we obtained two-dimensional trajectories for each individual fish (panel **b**). This permits the construction of a stochastic time-series for the group alignment, or polarisation $\boldsymbol{M}(t)$ [see Eq. (1)]. For $|\boldsymbol{M}| \approx 1$ the fish are moving in a coherent direction, whereas for $|\boldsymbol{M}| \approx 0$, there is no prevailing direction and the shoal is effectively isotropic (panel **c**).

I. EXPERIMENTAL SETUP

Our experiments involved filming schools of freshwater juvenile *E. suratensis* in a large laboratory tank that was sufficiently shallow as to constrain motion to two dimensions [Fig. 1 and Supplementary Section I]. We focussed on small-to-medium sized groups— $N = 15$, $N = 30$, and $N = 60$— which ensured that schools were localised, with a spatial extent that was only a fraction of the overall tank size (see Supplementary Sections II and III, respectively, for details concerning larger schools and controls for the effects of the tank boundary).

Each group size was recorded for approximately 3.5 hours in total, across four separate trials for $N = 15$, 30, and three separate trials for $N = 60$. The temporal resolution was one frame every 0.04 s. However, at this timescale, movement is intermittent and the fish frequently stop and start, making it hard to discern a direction of motion. We therefore consider only one frame in every three— that is, every $\delta t = 0.12$ s. Using particle tracking, we extract the two-dimensional velocities $\boldsymbol{v}_i(t_n) = [\boldsymbol{x}_i(t_n + \delta t) - \boldsymbol{x}_i(t_n)]/\delta t$, where the index $i = 1, 2, \ldots, N$ labels fish, and the time increments are given by $t_n = n\,\delta t$, for $n = 0, 1, 2, \ldots$ *etc*.

At the individual level, the direction of motion of the i-th fish (at time t_n) is just $\hat{\boldsymbol{v}}_i(t_n) = \boldsymbol{v}_i(t_n)/|\boldsymbol{v}_i(t_n)|$. At the group level, both the direction and degree of the fish alignment are encapsulated by a vector order parameter, often referred to as the group polarisation

$$\boldsymbol{M}(t_n) = \frac{1}{N}\sum_{i=1}^{N} \hat{\boldsymbol{v}}_i(t_n). \qquad (1)$$

When $|\boldsymbol{M}|$ is close to 1, the fish are moving in a coherent direction, whereas when $|\boldsymbol{M}|$ is close to zero, there is no prevailing direction and individual motion is isotropic (see Fig. 1).

II. SCHOOLING INCREASES AS GROUP SIZE DECREASES

At each group size, the steady-state statistics of the school's polarisation are well represented by constructing histograms over the entire time-series (Fig. 2, panels **a**-**f**).

For $N = 60$, the most likely configuration is around $\boldsymbol{M} = \boldsymbol{0}$, which corresponds to motion that is isotropic and disordered (Fig. 2, panel **f**). For $N = 30$, this isotropic peak is still present in the histogram, but reduced, and an annulus of high frequencies can be seen where $|\boldsymbol{M}| \approx 1$, which corresponds to highly aligned motion (Fig. 2, panel **e**). For $N = 15$, the highest frequency values are near the highly-aligned $|\boldsymbol{M}| \approx 1$ annulus, with only a small isotropic bump at the centre (Fig. 2, panel **d**).

Regardless of group size, the statistics have angular symmetry, indicating that there is no preferred direction of schooling, as expected. Considering only the magnitude of the polarisation (Fig. 2, panels **g**-**i**), the likelihood of observing isotropic motion relative to that of ordered motion is revealed to be almost negligible, despite the central peaks observed in panels **d**-**f**. More importantly, the relative likelihood of observing fish with highly aligned motion *increases* as N *decreases*, which is also supported by visual inspection of the underlying trajectories (Fig. 2, panels **a**-**c**).

In the following, via analyses of stochastic dynamics as well as controls for confounding effects of boundaries of the tank (Supplementary Section III), we find that both the likelihood of schooling, and its group-size dependence, bear all the features of a finite-size noise-induced phenomenon.

III. SCHOOLING IS A FINITE-SIZE NOISE-INDUCED EFFECT

To understand the dynamical context of our observations, it is helpful to extract autocorrelation functions for the group polarisation components M_x and M_y (Methods Section I A & Extended Data Figure 1). The results are qualitatively simi-

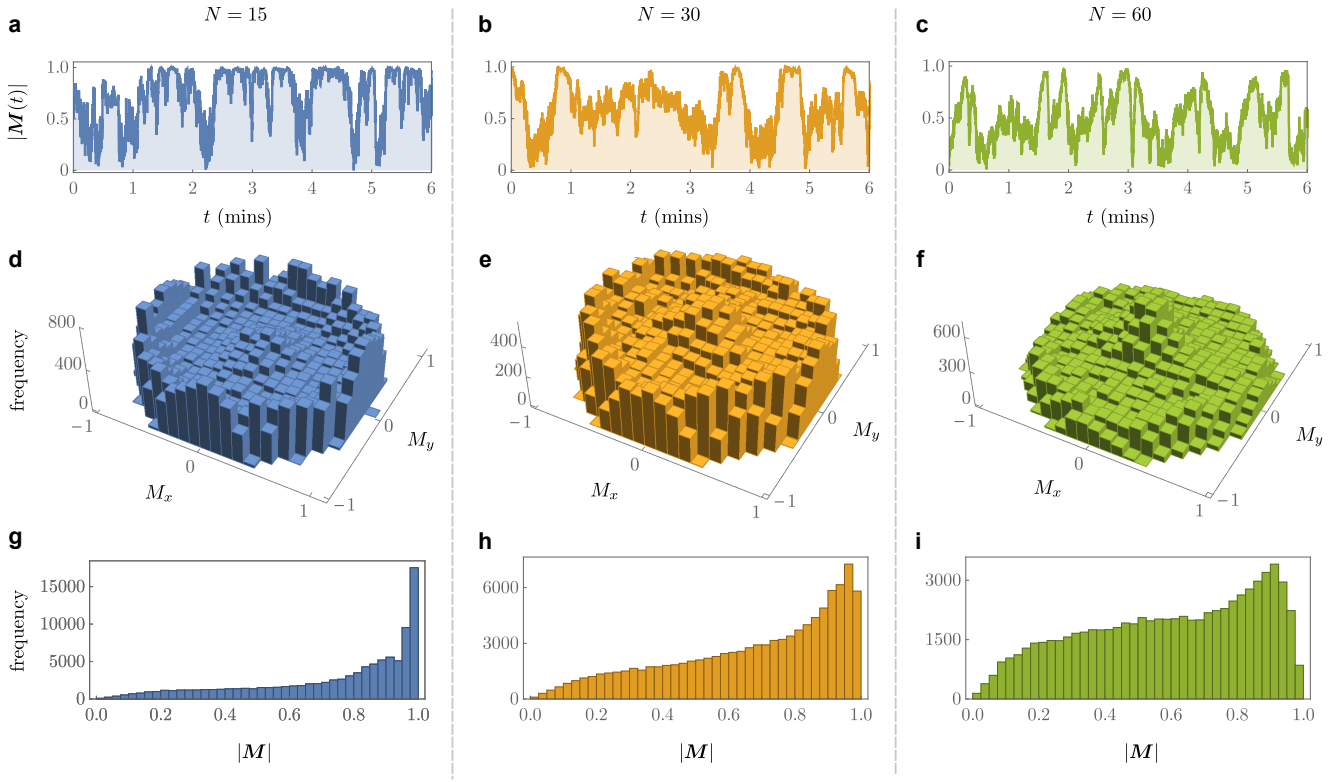

FIG. 2. **Steady-state statistics demonstrate high degree of schooling**. A visual inspection of representative trajectories $|\boldsymbol{M}(t)|$ indicates that, as group size decreases, fish motion becomes increasingly ordered (panels **a**-**c**). Histograms of $\boldsymbol{M}$ reveal there is no preferred direction of motion (panels **d**-**f**). Taking account of this angular symmetry, panels **g**-**i** confirm that schooling is indeed the most likely behaviour, and that the smaller the group's size the greater the relative likelihood of such highly ordered motion. Results are independent of the time-interval over which the histograms are constructed, so long as it is substantially larger than the correlation time.

lar to exponentially-damped cosines, indicating the presence of two characteristic time-scales: one for the short-time decay of correlations to zero, and the other for the decaying envelope of longer-time oscillatory behaviour. The latter appears to be consistent with the effects of finite tank size—on average, the speed of the fish is $\approx 6\,\mathrm{cm\,s^{-1}}$ which, given a tank diameter of 180 cm, implies a time-scale of approximately 30 s, in-line with the observed range of 20-50 s. We therefore focus on the shorter time-scale, whose mean value (across all experiments) is $\Delta t \approx 5.9$ s. This, we assert, captures correlations (and their decay) due to any underlying local interactions that result in the alignment of fish.

On the time-scale Δt, we further assume (and later confirm) that the dynamics of alignment is well-approximated by a stochastic differential equation (SDE), of the type that arises from system-size expansions of transition rates [14] and is synonymous with steady-state statistics that are N-dependent. Usually, such mesoscopic SDEs are constructed formally by coarse-graining known 'microscopic' rules. However, in the context of collective animal motion, the rules describing individual behavioural interactions are typically unknown. We therefore quantify the mesoscopic dynamics directly from the data, and then later infer microscopic rules by comparison with both theory and computer simulations.

Consigning the details to Methods Section I B, we construct an Itô-sense SDE from our data, which is of the general form

$$\frac{d\boldsymbol{m}}{dt} = \boldsymbol{A}(\boldsymbol{m}) + \mathsf{B}(\boldsymbol{m}) \cdot \boldsymbol{\eta}(t), \tag{2}$$

where $\boldsymbol{m}(t) \in \mathbb{R}^2$, bold typeface is used for two-dimensional vectors and sans-serif for a rank-2 tensor. The elements of the vector $\boldsymbol{\eta}$ are independent sources of Gaussian white noise, such that $\langle \eta_j(t) \rangle = 0$ and $\langle \eta_j(t)\, \eta_k(t') \rangle = \delta_{jk}\, \delta(t-t')$ for $j,k = 1,2$ (angle brackets indicates an average over stochastic realisations).

In principle, the components of the deterministic part of Eq. (2) can be found by numerically extracting the first jump moment(s) from the data. Similarly, the components of the stochastic part can also be obtained by extracting the second jump moment(s), which are given by $\sum_k B_{jk} B_{lk}$ (where B_{jk} are the components of B). In practice, however, this requires smooth interpolations, or 'best fits'. Guided by exactly solvable one-dimensional toy models ([13, 17] and Supplementary Section IV) we propose and test different functional forms, each dependent on N, $\boldsymbol{m}$, and other unspecified parameters. Using a simple least-squares procedure to fit the free parameters, we then choose expressions with the greatest adjusted-R^2, being careful to avoid over-fitting (Fig. 3).

Substituting the resulting functions into Eq. (2), we ob-

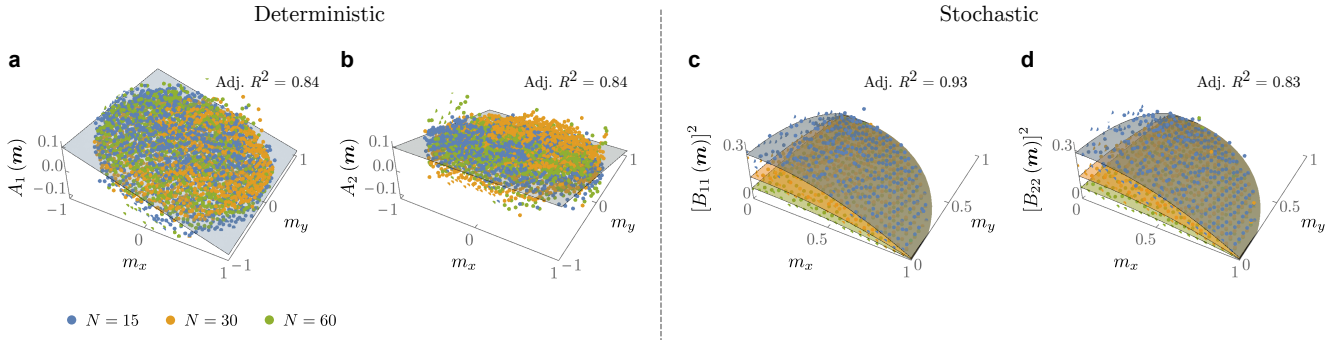

FIG. 3. **Empirical fitting of the first and second jump-moments reveals that schooling is noise induced**. The first and second jump-moments are extracted systematically from the data. The first jump-moments (panels **a** and **b**) correspond to the components A_i that characterise the school's deterministic behaviour in the $N \to \infty$ limit [*cf.* Eq. (2)]. Both A_1 and A_2 display a shallow linear slope with gradient ≈ -0.1 and zero intercept, the former in the m_x direction, and the latter in the m_y direction. This corresponds to a weak pull towards isotropic, disordered motion (*i.e.*, $\boldsymbol{m} = \mathbf{0}$), irrespective of group size. The second jump-moments (panels **c** and **d**) are related to the multiplicative prefactors, B_{ij} [*cf.* Eq. (2)]. Both B_{11} and B_{22} are symmetric around, and maximal at, $\boldsymbol{m} = \mathbf{0}$, decreasing towards zero for values $|\boldsymbol{m}| \gtrsim 1$. The magnitude of the noise is therefore largest at the stable fixed point ($\boldsymbol{m} = \mathbf{0}$) of the deterministic dynamics, which gives rise to noise-induced behaviour. Moreover, the the second jump moments scale as $O(1/\sqrt{N})$— *i.e.*, they increase as group size decreases— which is a signature of *intrinsic* noise. The cross-correlations B_{12} and B_{21} (not shown) are distributed randomly around zero with no trend.

tain

$$\frac{d\boldsymbol{m}}{dt} = -\alpha\,\boldsymbol{m} + \left[\frac{\beta\left(1-|\boldsymbol{m}|^2\right)+\alpha}{N}\right]^{1/2} 1\cdot\boldsymbol{\eta}(t), \qquad (3)$$

where 1 is the two-dimensional identity matrix, and the constants $\alpha = 0.1$ and $\beta = 4.0$ have been determined by the fitting procedure. Reassuringly, direct Milstein-method numerical integration of Eq. (3) recovers steady-state statistics that retain the key features of our experimental observations (Methods Section III A & Extended Data Figure 2).

Of note, we see that B is $O(1/\sqrt{N})$, whilst $\boldsymbol{A}$ is $O(\text{constant})$, which confirms our earlier assumption and implies that the noise is likely *intrinsic*, due to probabilistic interactions between a finite number of individuals. Moreover, in the deterministic $N \to \infty$ limit, the single stable fixed point of Eq. (3) is at $\boldsymbol{m} = \mathbf{0}$, which corresponds to isotropic disordered motion. This further implies that the observed high levels of ordering are in fact *noise-induced*, arising from the interplay between the deterministic and multiplicative-noise terms.

Informally, Eq. (3) can be understood in terms of the following heuristic; although the deterministic dynamics 'pulls' the system towards isotropic motion, the closer it gets, the larger the noise becomes, therefore 'kicking' the system away, towards more aligned motion. Conversely, the more aligned the motion, the smaller the fluctuations, and the longer the system is able to reside there.

IV. A PAIRWISE COPYING MODEL CAPTURES KEY FEATURES OF DATA

Our analysis implies behaviour that is reminiscent of individual-based binary-choice models that appear in the literature (*e.g.* [17]). By introducing continuous degrees of freedom, we invoke a simple two-dimensional extension of such models— similar to [21]— which extends voter model of opinion dynamics and makes notional contact with the mean-field XY model.

We assume that at each instant in time, t, the direction of each fish

$$\hat{\boldsymbol{d}}_i(t) = \begin{pmatrix}\cos\theta_i(t)\\ \sin\theta_i(t)\end{pmatrix}, \qquad (4)$$

is, itself, prescribed by a stochastic protocol for the dynamics of the angles $\theta_i(t)$ $(i = 1,\ldots,N)$. Using the notation of chemical reaction kinetics, we write down two competing types of underlying behaviour.

First, at a constant rate per unit time, s, every fish can spontaneously change its direction (angle). That is

$$\theta_i \xrightarrow{s} \theta_i + \mathcal{N}_{\text{trunc}}\left(0,\varepsilon,-\pi,\pi\right), \qquad (5)$$

where $\mathcal{N}_{\text{trunc}}\left(\mu,\sigma^2,a,b\right)$ is a truncated normal distribution with mean μ and variance σ^2, normalised over the interval (a,b).

Second, at a different rate, c, a given fish 'i' chooses another fish 'j' randomly and copies it— *i.e.*, it turns to move in the same direction:

$$\theta_i + \theta_{j\neq i} \xrightarrow{c} 2\theta_j. \qquad (6)$$

This second equation describes a pairwise interaction, and assumes that the system is 'mean-field' or 'fully-connected'; an assumption that we revisit in the *Discussion*.

Leaving the details of analytical calculations to Methods Section II, a Fourier-space system-size expansion can be used to demonstrate that, for finite N, such microscopic rules result in a stochastic dynamics for $\boldsymbol{m}$ that is described *precisely* by Eq. (3), so long as we make the identifications $\alpha = s\left(1-e^{-\varepsilon/2}\right)$ and $\beta = c$.

At the microscopic scale, the implication is that fish copy the orientation of other fish, one at a time, at a rate $c = 4$

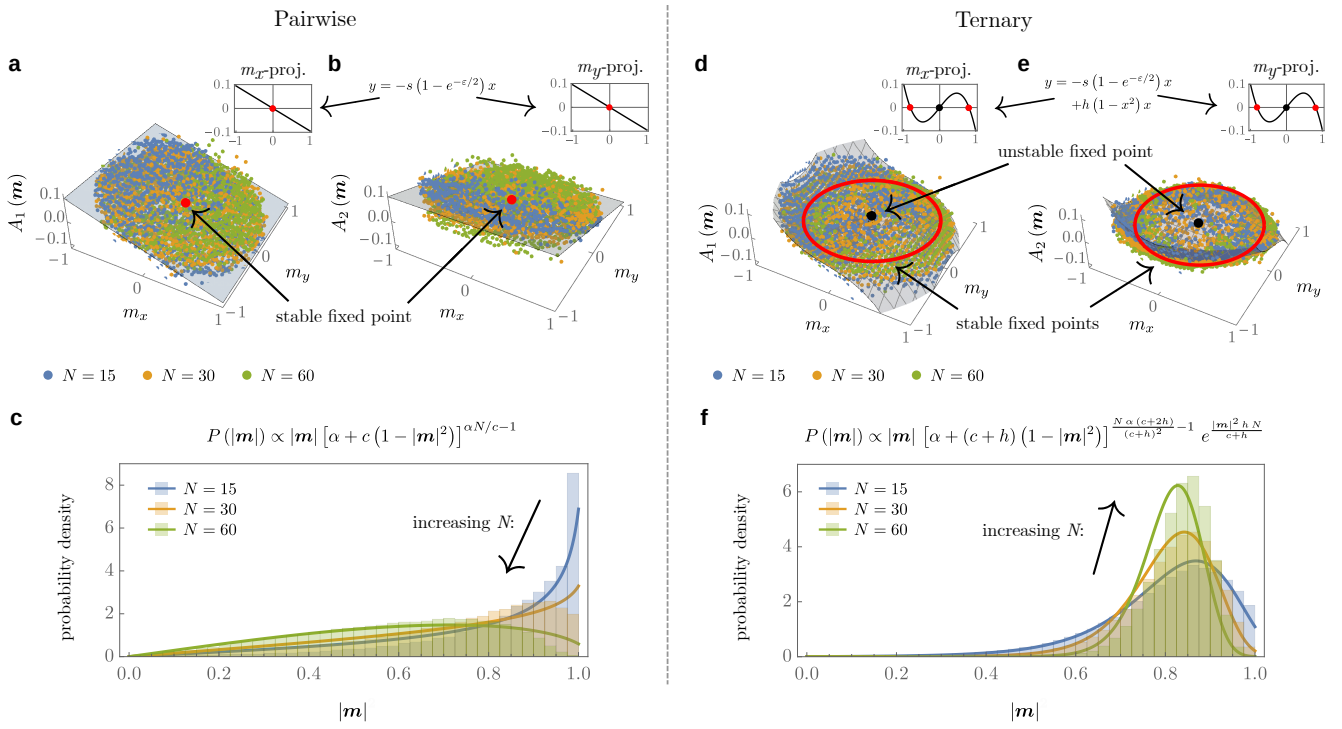

FIG. 4. **Pairwise vs. ternary interactions: theory and stohastic simulations**. Illustrative comparison between a pairwise model [*i.e.*, Eqs. (5) and (6) with $s = 0.25, \varepsilon = \pi/3$ and $c = 4$] and a ternary model [including the extra reaction defined by Eqs. (7) and (8), where $s = 0.25$, $c = 0.01$ and $h = 0.3$]. Data points in panels **a**, **b**, **d** and **e**, and histograms in panels **c** and **f**, are generated by Gillespie simulation. Surfaces and their sections (inset) in panels **a**, **b**, **d** and **e**, and lines in panels **c** and **f**, are taken from theory (Methods Section II). Whilst in both cases, theory agrees with simulations, only the pairwise model (panels **a** and **b**) reproduces the observed deterministic pull towards isotropic motion— *i.e.*, $\boldsymbol{m} = \boldsymbol{0}$ (*cf.* Fig. 3, panels **a** and **b**). For the ternary model, isotropic motion is an unstable fixed point, and a new line of (Lyapounov-)stable fixed points is introduced at finite $|\boldsymbol{m}|$ (panels **d** and **e**). As a result, the N-dependence of the steady-state PDFs generated from the pairwise model closely resembles that derived from the data, whilst the ternary model does not (panels **c** and **f**). The stochastic part of both the pairwise and the ternary models are qualitatively similar in the functional forms as predicted by theory (see Extended Data Figure 3).

times a second. From the value of α ($= 0.1$) per second, however, we cannot disentangle the rate of spontaneous directional switching (s) and the amplitude of the resulting directional change (ε). We remark that, often, copying interactions may only lead to a micro-adjustment of a fish's direction of motion, since schools are most likely found in a highly polarised state where any two fish are already broadly aligned. To put these into context, similar interaction rates were observed in free-swimming golden shiners (*Notemigonus crysoleucas*) [22].

At the mesoscopic scale [i.e. Eq. (3)], this suggests that the non-trivial alignment-driving part of the multiplicative noise in the data arises solely from the voter-like copying behaviour [Eq. (6)], whilst the deterministic pull towards isotropic motion is due to spontaneous direction switching [Eq. (5)].

V. HIGHER-ORDER INTERACTIONS ARE SUB-DOMINANT

Although the agreement between data and aforementioned analysis makes a strong case for a pairwise copying model [Eqs. (5) and (6)], it is important to rule out the possible role of higher-order interactions. Again drawing inspiration from simple models (see *e.g.*, [13, 23] and Supplementary Section IV), we propose the following ternary extension, to be included alongside interactions defined by Eqs. (5) and (6):

$$\theta_i + \theta_{j\neq i} + \theta_{\substack{k\neq i\\ \neq j}} \xrightarrow{h} \begin{cases} 2\theta_\ell + \theta_{\ell'} \\ 2\theta_m + \theta_{\ell'} \end{cases}, \tag{7}$$

where

$$\left\{\ell, \ell'\right\} = \underset{\{\{p,q\}\subset\{i,j,k\}\}}{\arg\min} \left(\min\left(2\pi - \left|\theta_p - \theta_q\right|, \left|\theta_p - \theta_q\right|\right)\right). \tag{8}$$

That is, with a specific rate h, three individuals are picked at random and their directions are compared in order to find which pair have the minimum (acute) angular difference. The remaining individual then turns to copy either of the two others with equal probability.

As with the pairwise case, the finite-N SDE that corresponds to this ternary extension can also be derived using a system-size expansion of the relevant Master equation in Fourier-space, although in this case, the calculation requires an additional assumption to ensure moment-closure.

The differences between the two cases (pairwise and ternary) are very clear (Fig. 4 and Methods Section II):

ternary interactions add a term $h(1-|\boldsymbol{m}|)\boldsymbol{m}$ to the deterministic ($N\to\infty$) dynamics, significantly altering the N-dependence of the steady-state PDF. In particular, if h is sufficiently high, then the isotropic $\boldsymbol{m}=\boldsymbol{0}$ fixed point switches from being stable to unstable, and a line of new (Lyapunov-)stable fixed points appears at finite $|\boldsymbol{m}|$, meaning ordering is not lost as N increases. Instead, the steady-state probability distribution simply becomes increasingly peaked around the finite-$|\boldsymbol{m}|$ stable fixed point(s) associated with ternary interactions.

By contrast, if h is sufficiently low that the fixed points of the deterministic dynamics remain unchanged, then ternary interactions are sub-dominant and the group-level behaviour essentially replicates that described for the pairwise only case. That is, we cannot unambiguously rule out weak ternary, or indeed higher order interactions of any other type. Nevertheless, the observed N-dependent ordering does appear to be clear evidence that the dominant mode of interaction is pairwise; involving only two fish, to the exclusion of all others (including local averaging).

The intuition provided by the above comparison is backed-up by more systematic simulations and model fitting to the data. Specifically, we simulated both generalisations of Eqs. (7) and (8) *and* a mean-field Vicsek model (the latter to explicitly rule out any effects arising from averaging), each of which included up to five-body interactions. Then, using a Genetic Algorithm in the context of repeated Gillespie simulations, we optimised the rates of such many-body interaction models against the experimental data (Methods Section III B-D). Specifically, we minimized the Kullback-Leibler divergence between the simulation-generated steady state PDFs, and those extracted from the experimental data— *i.e.,* by normalising the histograms in Fig. 2, panels **g**, **h** & **i**. In all cases, we found that the model most consistent with the data had a dominant mode of interaction that was pairwise— *i.e.*, the rates corresponding to higher-order interactions were negligible (see Extended Data Tables 1 & 2).

VI. DISCUSSION

In summary, we report rare empirical evidence of noise-induced schooling in fish due to finite-size effects— serving to underline not only the importance of intrinsic noise, but also how it can manifest at the collective level as a multiplicative noise pre-factor. In particular, our results have implications for the possible modes of interaction between fish, and what features these must have in order to give rise to such behaviour.

We put forward a microscopic model which, although simple, convincingly reproduces our data. Both analytical work and stochastic simulations match not only the emergent finite-N steady-state statistics, but also the nature of the jump-moments, and therefore the aforementioned noise-induced character. The model involves two types of behaviour: individuals can either spontaneously change direction, or copy another individual, chosen at random. Importantly, this requires, at most, *pairwise* alignment interactions, where a given fish only interacts with other fish, one at a time. Models with dominant higher-order interactions, including local-averaging, do not represent the data well. The reasons for this can be seen in the provided example of a ternary interaction[1] whereby the deterministic dynamics is changed in a way reminiscent of the difference between quadratic and quartic potentials: a previously stable isotropic fixed point becomes unstable, and a line of new fixed points emerges at large polarisations, resulting in dynamical behaviour that is dramatically different from the data.

Notably, the conclusion of a pairwise interaction is broadly in-line with Refs. [5, 8] which concern very small groups of fish ($N\leq 5$), characterising correlations in turning angles, implied forces, and directions, respectively. However, in those studies, the pairwise interactions are highly likely to be between nearest neighbours, suggesting an apparent conflict with our mean-field approach. Reassuringly, for schools such as those in our experiments— *i.e.,* small, localised, and with high levels of alignment— both the data and explicitly spatial simulations indicate that, in fact, there is sufficient 'configuration space' mixing that a mean-field description is indeed a good approximation. That is, over time, repeatedly sampling the directions of fish in a given local neighbourhood is well-approximated, statistically, by sampling at random from the entire school (see Supplementary Section V A and B, respectively).

Moreover, there is evidence to suggest that any putative interplay between alignment, individual speed and other factors, such as the boundary, are neither in conflict with, nor offer an alternative explanation for, our observations. Crucially, we find that *i*) the structure of the jump-moments— and hence the intrinsic-noise-induced character— are very robust to the removal of data pertaining to the boundary (Supplementary Section III A), and *ii*) there is no appreciable change with group size in the overall statistics of either individual speeds (Supplementary Section III B) or nearest-neighbour separations. Taken together, and barring pathological cases, this counters the possibility of any straightforward leading-order mechanism for the alignment of *E. Suratensis*, other than that induced by intrinsic noise.

In the context of analysing jump-moments, we draw comparisons with Ref. [13], which relates to the only other example where these techniques have been used in relation to collective motion: a study of locust nymphs moving around a quasi-1D track [10]. In that case, the interplay between the deterministic and multiplicative parts does *not* result in noise-induced ordering (*i.e.*, peaks in the probability distrubution that are away from the deterministic fixed points). The authors of [13] therefore describe the data by employing a ternary interaction whose behaviour, albeit in one dimension, is akin to Eqs. (7) and (8), which are described in Fig. 4. In this light, the two studies can be seen as evidence in support of a point alluded-to in the introduction; the proper analysis of jump-moments can act as an important

[1] We stress that we have simulated up to five-body interactions.

discriminating factor between different classes of behaviour and/or types of animal.

In conclusion, our study demonstrates the importance of noise due to probabilistic interactions between a finite number of individuals. This emphasises the need for a re-appraisal of traditional approaches to understanding collective motion. Looking forwards, the dual issues of space and density are the clear challenges ahead. In this article, we have begun to understand how the total number of individuals, N, in localised schools, and therefore perhaps density in de-localised schools, non-trivially impacts on the ordering dynamics. However, it is not clear *a priori* how the density within groups itself fluctuates, and to what extent those statistics are coupled to alignment. More generally, how can the rigorous derivation of multiplicative noise terms be incorporated into broader (spatial) active-hydrodynamic descriptions of collective motion [20, 24]? Some tentative theoretical steps have been made, notably in the context of the Vicsek model [25], active nematics [26] (extending previous work concerning passive Brownian particles [27]) and in one-dimensional models of direction-switching [28, 29]. However, approaches vary, and the techniques used are far from 'off the shelf' solutions. Crucially, no such empirical studies exist at present. From a biological perspective, it is well known that collective behaviour offers many advantages to organisms, with implications to their survival and fitness [30, 31]. Consequently, we are led to ask whether the simple pairwise copying interactions, and the resulting noise-induced schooling, may have novel evolutionary ramifications. We therefore welcome further work in these areas.

VII. AUTHOR CONTRIBUTIONS

VG conceived of, and oversaw the project. JJ, UA-K and HR performed experiments. JJ and RGM analysed and interpreted the data. JJ and MDR performed simulations. TR and RGM performed calculations. RGM wrote the manuscript, with input from JJ, MDR and VG. JJ and RGM contributed equally to the manuscript.

VIII. DECLARATION

The authors declare no conflict of interest.

IX. DATA AVAILABILITY STATEMENT

All data and codes including readme files necessary to reproduce Figs 2-4 are available via Git-hub: `https://github.com/tee-lab/schooling_fish`.

X. CORRESPONDENCE

Correspondence regarding the manuscript may be addressed to `guttal@iisc.ac.in`, `jiteshjhawar@gmail.com`, `r.g.morris@unsw.edu.au`, `dannym@iisc.ac.in`.

XI. ACKNOWLEDGEMENTS

VG thanks C Jayaprakash for introducing him to the fascinating world of noise-induced phenomena. We acknowledge assistance from Subhakar Chakraborty, Elsa Mini Jos, Arshed Nabeel and Tapan Goel. We thank Binoy V V for suggestions on schooling fish species native to India and their hatcheries. We also thank S. Ramaswamy for a critical reading of the manuscript and Christos C Ioannou for discussions. JJ acknowledges support by the CSIR, India for research scholarship. RGM acknowledges both the Simons Foundation (USA) and EMBL-Australia for funding. MDR acknowledges DST India INSPIRE faculty award for funding. TR acknowledges the Royal Society (UK) for funding. VG acknowledges support from DBT-IISc partnership program, SERB (DST) and infrastructure support from DST-FIST.

[1] Ballerini, M. et al. Interaction ruling animal collective behavior depends on topological rather than metric distance: Evidence from a field study. *Proc. Natl. Acad. Sci.*, **105,** 1232–1237 (2008).

[2] Bialek, W. et al. Statistical mechanics for natural flocks of birds. *Proc. Natl. Acad. Sci.*, **109,** 4786–4791 (2012).

[3] Pearce, J. G. D., Miller, A. M., Rowlands, G., and Turner, M. S. Role of projection in the control of bird flocks. *Proc. Natl. Acad. Sci.*, **111,** 10422–10426 (2014).

[4] Becco, C., Vandewalle, N., Delcourt, J., and Poncin, P. Experimental evidences of a structural and dynamical transition in fish school. *Phys. A Stat. Mech.*, **367,** 487–493 (2006).

[5] Herbert-Read, J. E. et al. Inferring the rules of interaction of shoaling fish. *Proc. Natl. Acad. Sci.*, **108,** 18726–18731 (2011).

[6] Gautrais, J. et al. Deciphering interactions in moving animal groups. *PLoS Comput. Biol.*, **8,** e1002678 (2012).

[7] Ward, A. J. et al. Local interactions and global properties of wild, free-ranging stickleback shoals. *R. Soc. Open Sci.*, **4,** 170043 (2017).

[8] Jiang, L. et al. Identifying influential neighbors in animal flocking. *PLOS Comput. Biol.*, **13,** 1–32 (2017).

[9] Buhl, J. et al. From disorder to order in marching locusts. *Science*, **312,** 1402–1406 (2006).

[10] Yates, C. A. et al. Inherent noise can facilitate coherence in collective swarm motion. *Proc. Natl. Acad. Sci.*, **106,** 5464–5469 (2009).

[11] Shemesh, Y. et al. High-order social interactions in groups of mice. *Elife*, **2,** e00759 (2013).

[12] Rands, S. A., Hayley, M., and Terry, N. L. Red deer synchronise their activity with close neighbours. *PeerJ*, **2,** e344

(2014).
[13] Dyson, L., Yates, C. A., Buhl, J., and McKane, A, J. Onset of collective motion in locusts is captured by a minimal model. *Phys. Rev. E*, **92,** 052708 (2015).
[14] Van Kampen, N. G. *Stochastic Processes in Physics and Chemistry.* (Elsevier, Amsterdam, 1992).
[15] Horsthemke, W., and Lefever, R. *Noise-Induced Transitions: Theory and Applications in Physics, Chemistry and Biology*. (Springer, Berlin 1984).
[16] Ridolfi, L., D'Odorico, P., and Laio, F. *Noise-Induced Phenomena in the Environmental Sciences*. (Cambridge University Press, New York, 2011).
[17] Biancalani, T., Dyson, L., and McKane, A. J. Noise-induced bistable states and their mean switching time in foraging colonies. *Phys. Rev. Lett.*, **112,** 038101 (2014).
[18] Boettiger, C. From noise to knowledge: how randomness generates novel phenomena and reveals information. *Ecol. Lett.*, **21,** 1255–1267 (2018).
[19] Vicsek, T., Czirók, A., Ben-Jacob, E., Cohen, I., and Shochet, O. Novel type of phase transition in a system of self-driven particles. *Phys. Rev. Lett.*, **75,** 1226–1229 (1995).
[20] Toner, J., and Tu, Y. Long-range order in a two-dimensional dynamical xy model: how birds fly together. *Phys. Rev. Lett.*, **75,** 4326–4329 (1995).
[21] Baglietto, G., and Vazquez, F. Flocking dynamics with voter-like interactions. *J. Stat. Mech.*, **2018,** 033403 (2018).
[22] Rosenthal, S. B., Twomey, C. R., Hartnett, A. T., Wu, H. S., and Couzin, I. D. Revealing the hidden networks of interaction in mobile animal groups allows prediction of complex behavioral contagion. *Proc. Nat. Acad. Sci. USA*, **112,** 4690–4695 (2015).
[23] Jhawar, J., Morris, R. G., and Guttal, V. Deriving mesoscopic models of collective behavior for finite populations. in *Handb. Stat. Integr. Popul. Biol. Model.*, (eds. Rao, A. S. R. S., & Rao, C. R.) **40,** 551–594 (Elsevier, Amsterdam, Netherlands, 2018).
[24] Ramaswamy, S. The mechanics and statistics of active matter. *Annu. Rev. Condens. Matter Phys.*, **1,** 323–45 (2010).
[25] Barré, J., Chétrite, R., Muratori, M., and Peruani, F. Motility-induced phase separation of active particles in the presence of velocity alignment. *J. Stat. Phys.*, **158,** 589–600 (2015).
[26] Bertin, E. et al. Mesoscopic theory for fluctuating active nematics. *New J. Phys.*, **15,** 085032 (2013).
[27] Dean, D. S. Langevin equation for the density of a system of interacting langevin processes. *J. Phys. A. Math. Gen.*, **29,** L613 (1996).
[28] Laighléis, E. Ó., Evans, M. R., Blythe, R. A. Minimal stochastic field equations for one-dimensional flocking. *Phys. Rev. E*, **98,** 062127 (2018).
[29] Chatterjee, P., and Goldenfeld, N. Three-body interactions drive the transition to polar order in a simple flocking model. *Phys. Rev. E*, **100,** 040602 (2019).
[30] Sumpter, D. J. *Collective Animal Behavior.* (Princeton University Press, 2010).
[31] Ioannou, C. C., Guttal, V., and Couzin, I. D. Predatory fish select for coordinated collective motion in virtual prey. *Science*, **337,** 1212–1215 (2012).

METHODS

I. EXTRACTION OF SDE FROM DATA

From the time series of group polarisation data, we first compute autocorrelation time and then extract the first and second jump moments. We refer the readers to [32] for a less technical presentation and justification of the method using numerical simulations; there, we also discuss how the structure of jump-moments can be used to infer local interactions, providing a complementary approach to existing methods such as those described in [6, 33–36].

A. Autocorrelation time

For each group size ($N = 15$, 30 and 60) we calculate the auto-correlation of the time-indexed quantities $M_x(t_n)$, $M_y(t_n)$ and $|\boldsymbol{M}(t_n)|^2$, where $t_n = n\,\delta t$, for all $n = 1, \ldots, \mathscr{N}$. We use the generic form

$$R(X,\Delta t) := \rho_{X,X}(\Delta t) = \frac{\langle (X_t - \mu)(X_{t+\Delta t} - \mu)\rangle}{\sigma^2}, \qquad (9)$$

where X represents a set of $\mathscr{N}$ time-indexed measurements with mean $\mu = \sum_t X_t/\mathscr{N}$, and variance $\sigma^2 = \sum_t (X_t - \mu)^2/\mathscr{N}$. The results are shown in Extended Data Figure 1.

For the case of M_x and M_y, the auto-correlation decays in an oscillatory manner (panels **a**-**f**). We are therefore able to extract two characteristic times. As argued-for in Section III, the time-scale of behavioural interactions is approximated by fitting $\exp(-\Delta t/\tau)$ to the initial decay of the auto-correlation function, truncated where it first crosses zero. We also fitted the envelope of the decay $[\exp(-\Delta t/\tau_{\rm env})]$ which we associate with the long-time correlations induced by finite tank size.

For the case of $|\boldsymbol{M}|^2$, the auto-correlation function is only weakly oscillatory, but appears to decay to a finite value as δt becomes large. We again attribute this to finite tank-size induced correlations, and find a characteristic decay time by fitting $\exp\left(-\Delta t/\tau_{|\boldsymbol{M}|^2}\right) + \mathscr{C}$, where both $\tau_{|\boldsymbol{M}|^2}$ and $\mathscr{C}$ are now fit-parameters.

B. Extracting jump-moments

With a formal basis in the system-size expansion of Master equations [14, 37], our basic assumption is that the data is well represented by an SDE of the form

$$\frac{dm_i}{dt} = A_i(\boldsymbol{m}) + \sum_{j=1}^{2} B_{ij}(\boldsymbol{m})\,\eta_j,\ \forall\ i = 1,2, \qquad (10)$$

which is just a component-wise version of Eq. (2). The coefficients A_i and B_{ij} are related to the first- and second-jump-moments— $a_i^{(1)}$ and $a_{ij}^{(2)}$, respectively— via:

$$a_i^{(1)} = A_i \text{ and } a_{ij}^{(2)} = \sum_{k=1}^{2} B_{ik}B_{jk}, \qquad (11)$$

where the η_j are sources of delta-correlated Gaussian white noise with zero mean and unit variance [*i.e.*, $\langle \eta_j \rangle = 0$, and $\langle \eta_i(t)\,\eta_j(t') \rangle = \delta_{ij}\,\delta(t-t')$]. More precisely, we assume that the data $\{\boldsymbol{M}(t_n) \in \mathbb{R}^2 : |\boldsymbol{M}(t_n)| \leq 1,\ t_n = n\,\delta t,\ \forall\ n = 1,\ldots,\mathscr{N}\}$ satisfies a *discretised* version of Eq. (10). Using the semi-formal notation prevalent within the physical sciences literature, we have

$$M_i(t_n+\Delta t) - M_i(t_n) = A_i\left(\boldsymbol{M}(t_n)\right)\Delta t + \sqrt{\Delta t}\sum_{j=1}^{2} B_{ij}\left(\boldsymbol{M}(t_n)\right)\eta_j(t_n), \tag{12}$$

where $\Delta t = \lambda\,\delta t$, for $\lambda \in \mathbb{Z}_+$ such that $1 \leq \lambda \leq \mathscr{N}$. At this stage, we may ask: what is the most appropriate value of λ over which to cleanly extract jump-moments? Dividing by Δt and taking an average over the $\mathscr{N}$ independent instances of the noise (one for each data point in the time-series) gives

$$\left\langle \frac{M_i(t_n+\Delta t) - M_i(t_n)}{\Delta t} \right\rangle_{\mathscr{N}} = A_i\left(\boldsymbol{M}(t_n)\right) + \frac{1}{\sqrt{\Delta t}}\sum_{j=1}^{2} B_{ij}\left(\boldsymbol{M}(t_n)\right)\left\langle \eta_j \right\rangle_{\mathscr{N}}. \tag{13}$$

Importantly, we note that, since $\mathscr{N}$ is finite, then the average indicated by angle brackets, $\langle\cdot\rangle_{\mathscr{N}}$, is only a *sample* mean. That is, it is a stochastic variable itself, with a finite variance of $O(\mathscr{N})$. However, we may also see that $\delta t = T/\mathscr{N}$—*i.e.*, the smallest time-step in the system is just the total time period divided by the number of data points, $\mathscr{N}$. Therefore $\Delta t = \lambda T/\mathscr{N}$ and so

$$\mathrm{Var}\left[\left\langle \frac{M_i(t_n+\Delta t) - M_i(t_n)}{\Delta t} \right\rangle_{\mathscr{N}}\right] \sim \frac{1}{\lambda\,T}, \tag{14}$$

which simply shows that the variance of the stochastic variable given by the right-hand side of Eq. (13) is just inversely proportional to λ, and hence the size of the time-step Δt. Therefore, in order to obtain a good estimate for the function(s) A_i, the procedure is to use

$$A_i\left(\boldsymbol{m}\right) = \frac{1}{\Delta t}\left\langle M_i\left(t_n+\Delta t\right) - M_i\left(t_n\right)\right\rangle_{\boldsymbol{M}(t_n)=\boldsymbol{m}}, \tag{15}$$

but choose a value of λ that is large enough to minimise the noise arising from finite data whilst, at the same time, small enough to ensure Δt is less than the correlation time, τ (see Methods Section I A). We use $\Delta t = \bar{\tau}$, the average decay time, across all trials, associated with the first zero of the autocorrelation function of polarisation components M_x and M_y.

By contrast, extracting the coefficients B_{ij} is relatively straightforward, and we may use the small size of Δt to our advantage. Multiplying two copies of Eq. (12) together and dividing by Δt gives

$$\frac{\left(M_i(t_n+\Delta t) - M_i(t_n)\right)\left(M_j(t_{n'}+\Delta t) - M_j(t_{n'})\right)}{\Delta t} = \sum_{k=1}^{2} B_{ik}\left(\boldsymbol{M}(t_n)\right)\eta_k \sum_{\ell=1}^{2} B_{i\ell}\left(\boldsymbol{M}(t_{n'})\right)\eta_\ell + O\left(\sqrt{\Delta t}\right). \tag{16}$$

Using the property that $\langle \eta_i(t)\eta_j(t') \rangle = \delta_{ij}\,\delta(t-t')$ then implies that

$$\sum_{k=1}^{2} B_{jk}B_{\ell k}\left(\boldsymbol{m}\right) = \frac{1}{\Delta t}\left\langle \left[M_j\left(t_n+\Delta t\right) - M_j\left(t_n\right)\right] \times \left[M_\ell\left(t_n+\Delta t\right) - M_\ell\left(t_n\right)\right]\right\rangle_{\boldsymbol{M}(t_n)=\boldsymbol{m}}. \tag{17}$$

Here, in contrast to Eq. (15), which requires the effect of the variance of the sample mean $\langle \eta_j \rangle$ to be countered, the optimal value of Δt is just that which ensures the cleanest $O(\sqrt{\Delta t})$ cut-off, given the fixed sampling rate of the data. This is given by $\lambda = 1$, and corresponds to setting $\Delta t = \delta t$, where $\delta t = 0.12$s.

Finally, we note that there are two practical considerations which must also be taken into account. First, not all values $\boldsymbol{M}$ are present in the dataset, and hence the averages on the right-hand sides of the above expressions should be taken with respect to L small intervals: $\boldsymbol{m}_\Gamma \leq \boldsymbol{M}(t_n) \leq \boldsymbol{m}_\Gamma + \boldsymbol{\varepsilon}$, where $\{\boldsymbol{m}_\Gamma = \Gamma\boldsymbol{\varepsilon} : |\boldsymbol{\varepsilon}| \ll 1, \Gamma = 0,1,\ldots,L\}$. Secondly, the extracted jump-moments are likely noisy and it is typically necessary to find smooth interpolations, or 'best fits', by proposing and testing different functional forms, each dependent on N, $\boldsymbol{m}$, and other unspecified parameters.

II. DERIVATION OF MESOSCOPIC SDE IN TWO DIMENSIONS

A. Pairwise-interaction model

In contrast to the one-dimensional models described in the literature [17, 38, 39], analogous two-dimensional models pose a more significant challenge analytically, owing to their continuous degrees of freedom. Consider therefore, the stochastic protocol, or model, defined by Eqs. (5) and (6). Mindful of the calculation to come and without loss of generality, we *i*) replace the truncated Gaussian that appears in Eq. (5) with a wrapped Gaussian, and *ii*) permit self-copying. The resultant 'rules' are now

$$\begin{gathered}\theta_i \to \theta_i + \mu \pmod{2\pi}, \text{ with rate } r(\varepsilon) = \frac{s}{\sqrt{2\pi\varepsilon}}e^{-\mu^2/2\varepsilon}, \\ \text{and} \\ \theta_i \to \theta_j, \text{ with rate } c,\end{gathered} \tag{18}$$

where $\theta_i \in [0, 2\pi)$ for $i = 1\ldots N$. Write

$$\varphi(x) = \frac{1}{N}\sum_i \delta(x-\theta_i) \tag{19}$$

for the number density of fish as a function of their direction. The Master equation for the time evolution of the probability density $P(\varphi,t)$ is then given by

$$\frac{d}{dt}P(\varphi,t) = N\int_{-\pi}^{\pi}\mathrm{d}x\int_{-\pi}^{\pi}\mathrm{d}y\,\mathscr{Q}(\varphi;x,y)P(\varphi,t)\,, \qquad (20)$$

where

$$\mathscr{Q}(\varphi;x,y) = \left(\Delta_x^+\Delta_y^- - 1\right)\varphi(x)\left[r(x-y)+c\,\varphi(y)\right], \qquad (21)$$

such that $\Delta_x^{\pm}$ are creation/anihilation operators (acting on any expression that right-multiplies them). Next, we exploit the angular degrees-of-freedom and expand in Fourier series using the following conventions

$$f(x) = \frac{1}{2\pi}\sum_{k\in\mathbb{Z}} f_k e^{ikx}, \qquad f_k = \int_{-\pi}^{\pi} e^{-ikx}f(x)\mathrm{d}x\,. \qquad (22)$$

In Fourier space, the step operators can be expanded in large N [40], giving

$$\Delta_x^{\pm} = 1 \pm \frac{1}{N}\sum_k e^{-ikx}\frac{\partial}{\partial\varphi_k} + \frac{1}{2N^2}\sum_{k,\ell} e^{-i(k+\ell)x}\frac{\partial}{\partial\varphi_k}\frac{\partial}{\partial\varphi_\ell} + O\left(\frac{1}{N^3}\right). \qquad (23)$$

Ignoring $O\left(1/N^3\right)$ terms, it follows that

$$\left(\Delta_x^+\Delta_y^- - 1\right) = \frac{1}{N}\sum_k\left(e^{-ikx}-e^{-iky}\right)\frac{\partial}{\partial\varphi_k} + \frac{1}{2N^2}\sum_{k,\ell}\left(e^{-i(k+\ell)x}+e^{-i(k+\ell)y}-2e^{-ikx-i\ell y}\right)\frac{\partial}{\partial\varphi_k}\frac{\partial}{\partial\varphi_\ell}\,, \qquad (24)$$

and therefore

$$\varphi(x)\left[r(x-y)+c\,\varphi(y)\right] = \left(\frac{1}{2\pi}\right)^2\sum_{n,m}\left(\varphi_n r_m e^{inx+im(x-y)} + c\,\varphi_n\varphi_m e^{inx+imy}\right). \qquad (25)$$

Putting these together, and introducing $a_k = s(1-e^{-k^2\varepsilon/2})$, gives

$$\begin{aligned}\frac{d}{dt}P(\boldsymbol{\varphi},t) = &\\ &\sum_{k,n,m}\frac{\partial}{\partial\varphi_k}\left(\frac{1}{2\pi}\right)^2\int_{-\pi}^{\pi}\mathrm{d}x\int_{-\pi}^{\pi}\mathrm{d}y\left(e^{-ikx}-e^{-iky}\right)\\ &\left(\varphi_n r_m e^{inx+im(x-y)} + c\,\varphi_n\varphi_m e^{inx+imy}\right)P(\boldsymbol{\varphi},t)\\ &+\frac{1}{2N}\sum_{k,\ell,n,m}\frac{\partial}{\partial\varphi_k}\frac{\partial}{\partial\varphi_\ell}\left(\frac{1}{2\pi}\right)^2\int_{-\pi}^{\pi}\mathrm{d}x\int_{-\pi}^{\pi}\mathrm{d}y\\ &\left(e^{-i(k+\ell)x}+e^{-i(k+\ell)y}-2e^{-ikx-i\ell y}\right)\\ &\times\left(\varphi_n r_m e^{inx+im(x-y)} + c\,\varphi_n\varphi_m e^{inx+imy}\right)P(\boldsymbol{\varphi},t)\\ =&\sum_k\frac{\partial}{\partial\varphi_k}a_k\varphi_k P(\boldsymbol{\varphi},t) + \frac{1}{N}\sum_{k,\ell}\frac{\partial}{\partial\varphi_k}\frac{\partial}{\partial\varphi_\ell}\\ &\left[\frac{1}{2}\left(a_k+a_\ell-a_{k+\ell}\right)\varphi_{k+\ell} + c\left(\varphi_{k+\ell}-\varphi_k\varphi_\ell\right)\right]P(\boldsymbol{\varphi},t)\,.\end{aligned} \qquad (26)$$

Recognising that $|\boldsymbol{m}|^2 = \varphi_1\varphi_{-1} = |\varphi_1|^2$, we proceed by focussing on the dynamics of the first moment

$$\left\langle|\boldsymbol{m}|^2\right\rangle = \int\prod_{k=1}^{\infty}\mathrm{d}u_k\mathrm{d}v_k\,|\varphi_1|^2 P(\varphi,t)\,, \qquad (27)$$

where we use the notation that $u_k, v_k \in \mathbb{R}$ are just the real and imaginary parts of φ_k, respectively, and $P(\varphi,t) = P(\varphi_1,\varphi_2,\ldots,\varphi_n,t)$ by virtue of the aforementioned Fourier series. Using Eq. (26) and the fact that

$$\frac{\partial|\boldsymbol{m}|^2}{\partial\varphi_k} = \varphi_1\delta_{k,-1}+\varphi_{-1}\delta_{k,1} \quad \text{and} \quad \frac{\partial^2|\boldsymbol{m}|^2}{\partial\varphi_k\partial\varphi_\ell} = \delta_{k,-1}\delta_{\ell,1}+\delta_{\ell,-1}\delta_{k,1}\,, \qquad (28)$$

integration-by-parts may be used to show that

$$\begin{aligned}\frac{d}{dt}\langle|\boldsymbol{m}|^2\rangle = &\left\langle\sum_k|\boldsymbol{m}|^2\frac{\partial}{\partial\varphi_k}a_k\varphi_k\right.\\ &+\frac{1}{N}\sum_{k,\ell}|\boldsymbol{m}|^2\frac{\partial}{\partial\varphi_k}\frac{\partial}{\partial\varphi_\ell}\left[\frac{1}{2}\left(a_k+a_\ell-a_{k+\ell}\right)\varphi_{k+\ell}\right.\\ &\left.\left.+c\left(\varphi_{k+\ell}-\varphi_k\varphi_\ell\right)\right]\right\rangle\\ =&-2a\langle|\boldsymbol{m}|^2\rangle+\frac{2}{N}\left[a+c\left(1-\langle|\boldsymbol{m}|^2\rangle\right)\right].\end{aligned} \qquad (29)$$

where the shorthand $a = a_1 = a_{-1}$ has been used. Here, in contrast to solvable one-dimensional models, we resort to an ansatz: motivated by our data, we require that $\boldsymbol{m}$ obeys an autonomous and rotationally symmetric SDE of the form

of Eq. (3), which was initially obtained by fitting the empirically extracted jump moments from our experimental time-series data. That is,

$$\frac{d\boldsymbol{m}}{dt} = \boldsymbol{A}(\boldsymbol{m}) + \left[\frac{C(|\boldsymbol{m}|^2)}{N}\right]^{1/2} 1 \cdot \boldsymbol{\eta}(t)\,. \tag{30}$$

Using Itô's lemma and taking averages then implies that

$$\frac{d}{dt}\langle|\boldsymbol{m}|^2\rangle = 2\langle \boldsymbol{m}\cdot\boldsymbol{A}\rangle + \frac{2}{N}\langle C\rangle\,, \tag{31}$$

and therefore, comparing with Eq. (29), we must have $\boldsymbol{A} = -a\,\boldsymbol{m}$ and $C = a + c\left(1-|\boldsymbol{m}|^2\right)$, and hence

$$\frac{d\boldsymbol{m}}{dt} = -a\,\boldsymbol{m} + \sqrt{\frac{a+c\,(1-|\boldsymbol{m}|^2)}{N}}\,1\cdot\boldsymbol{\eta}(t)\,. \tag{32}$$

If we make the identifications $\alpha = a = s\left(1-e^{-\varepsilon/2}\right)$ and $\beta = c$, this is nothing other than Eq. (3), which was motivated by solvable one-dimensional models [see Eq. (8) of Supplementary Section IV].

Here, although the match between our model and the data cannot distinguish between fish that make small-and-frequent changes in direction and those that make large-and-infrequent changes, we suggest that such issues might be resolved by additional analyses of the type presented in [5, 8, 34], which consider correlations between individual trajectories in very small groups of fish ($N \leq 5$).

Furthermore, on the correspondence between one- and two-dimensional models, we remark that the extra prefactors present in (Supplementary Eq. (8)) can be informally accounted for by *i*) setting $\varepsilon = \pi$, and *ii*) noticing that a one-dimensional equivalent of *two* independent Gaussian noise sources with unit variance must carry an extra factor of $\sqrt{2}$ in the multiplicative noise term.

Finally, for completeness, the stationary distribution for $|\boldsymbol{m}|$ is, via recourse to the associated Fokker-Planck equation:

$$P(|\boldsymbol{m}|) \propto |\boldsymbol{m}|\left[a + c\left(1-|\boldsymbol{m}|^2\right)\right]^{aN/c-1}\,. \tag{33}$$

B. Ternary-interaction model

Consider adding ternary interactions, as described in Eqs. (7) and (8) of the main manuscript, to Eqs. (18). The resulting Master equation is

$$\begin{aligned}\frac{d}{dt}P(\varphi,t) = {}& N\int_{-\pi}^{\pi}\mathrm{d}x\int_{-\pi}^{\pi}\mathrm{d}y\,\mathscr{Q}(\varphi;x,y)P(\varphi,t)\\ &+N\int_{-\pi}^{\pi}\mathrm{d}x\int_{-\pi}^{\pi}\mathrm{d}y\int_{-\pi}^{\pi}\mathrm{d}z\,\mathscr{W}(\varphi;x,y,z)P(\varphi,t)\,,\end{aligned} \tag{34}$$

where $\mathscr{Q}$ is given by (21), and

$$\mathscr{W}(\varphi;x,y,z) = \begin{cases} 3h\left(\Delta_z^+\Delta_x^- - 1\right)\varphi(x)\varphi(y)\varphi(z) & \text{if } \|x-y\| < \min\left\{\|x-z\|,\|y-z\|\right\}\\ 0 & \text{otherwise.}\end{cases} \tag{35}$$

Here, $\|q\| = \min\{|q|, 2\pi-|q|\}$ denotes acute angluar distance. The rate function $\mathscr{W}$ represents choosing z from the distribution φ and having $z\mapsto x$ in the event that z is further from both x and y than they are from each other. We therefore compute the following integral over the support of $\mathscr{W}$, such that $\ell, m, n \in \mathbb{Z}$:

$$\begin{aligned}&\frac{3}{8\pi^3}\iiint_{\mathscr{W}>0} e^{i\ell x+imy+inz}\mathrm{d}z\,\mathrm{d}y\,\mathrm{d}x =\\ &\quad\frac{3}{8\pi^3}\int_{-\pi}^{\pi}\mathrm{d}x\int_{x-2\pi/3}^{x}\mathrm{d}y\int_{2x-y}^{2y-x+2\pi}\mathrm{d}z\,e^{i\ell x+imy+inz}\\ &\quad+\frac{3}{8\pi^3}\int_{-\pi}^{\pi}\mathrm{d}x\int_{x}^{x+2\pi/3}\mathrm{d}y\int_{2y-x}^{2y-x+2\pi}\mathrm{d}z\,e^{i\ell x+imy+inz}\\ &=\delta_{n,0}\,\delta_{m+\ell,0}\,\Gamma_\ell,\end{aligned} \tag{36}$$

where

$$\Gamma_\ell = \begin{cases} 1 & \text{if } \ell = 0\\ 0 & \text{if } \ell \text{ is non-zero and divides by 3}\\ 27/4\pi^2\ell^2 & \text{else.}\end{cases} \tag{37}$$

Using (36) in the context of (34) then gives

$$\begin{aligned}\frac{d}{dt}P(\boldsymbol{\varphi},t) = {}& \sum_k \frac{\partial}{\partial\varphi_k}a_k\varphi_k P(\boldsymbol{\varphi},t)\\ &+h\sum_k\frac{\partial}{\partial\varphi_k}\left(\varphi_k\sum_\ell\Gamma_\ell|\varphi_\ell|^2 - \sum_\ell\Gamma_\ell\varphi_\ell\varphi_{k-\ell}\right)P(\boldsymbol{\varphi},t)\\ &+\frac{1}{N}\sum_{k,k'}\frac{\partial}{\partial\varphi_k}\frac{\partial}{\partial\varphi_{k'}}\Big(\frac{1}{2}\left(a_k+a_{k'}-a_{k+k'}\right)\varphi_{k+k'}\\ &\qquad+c\left(\varphi_{k+k'}-\varphi_k\varphi_{k'}\right)\Big)P(\boldsymbol{\varphi},t)\\ &+\frac{h}{2N}\sum_{k,k'}\frac{\partial}{\partial\varphi_k}\frac{\partial}{\partial\varphi_{k'}}\sum_\ell\Gamma_\ell\Big(\varphi_{k+k'}|\varphi_\ell|^2\\ &\qquad+\varphi_\ell\varphi_{k+k'-\ell}-2\varphi_k\varphi_\ell\varphi_{k'-\ell}\Big)P(\boldsymbol{\varphi},t)\,.\end{aligned} \tag{38}$$

Again, we compute the dynamics of $\langle|\boldsymbol{m}|^2\rangle$; in this case

$$\begin{aligned}\frac{d}{dt}\langle|\boldsymbol{m}|^2\rangle &= -2a\langle|\boldsymbol{m}|^2\rangle + \frac{2}{N}\left[a + c\left(1-\langle|\boldsymbol{m}|^2\rangle\right)\right] \\ &+ \left\langle h|\boldsymbol{m}|^2 \sum_k \frac{\partial}{\partial\varphi_k}\Big(\varphi_k \sum_\ell \Gamma_\ell |\varphi_\ell|^2 \right. \\ &\left. - \sum_\ell \Gamma_\ell \varphi_\ell \varphi_{k-\ell}\Big)\right\rangle \\ &+ \left\langle |\boldsymbol{m}|^2 \frac{h}{2N} \sum_{k,k'} \frac{\partial}{\partial\varphi_k}\frac{\partial}{\partial\varphi_{k'}} \sum_\ell \Gamma_\ell \Big(\varphi_{k+k'}|\varphi_\ell|^2 \right. \\ &\left. + \varphi_\ell \varphi_{k+k'-\ell} - 2\varphi_k \varphi_\ell \varphi_{k'-\ell}\Big)\right\rangle \\ &= -2a\langle|\boldsymbol{m}|^2\rangle + \frac{2}{N}\left[a + c\left(1-\langle|\boldsymbol{m}|^2\rangle\right)\right] \\ &+ \left\langle -2h|\boldsymbol{m}|^2 \sum_\ell \Gamma_\ell |\varphi_\ell|^2 \right. \\ &\left. + h\sum_\ell \Gamma_\ell \varphi_\ell \left(\varphi_1\varphi_{-1-\ell} + \varphi_{-1}\varphi_{1-\ell}\right)\right\rangle \\ &+ \left\langle \frac{2h}{N}\sum_\ell \Gamma_\ell |\varphi_\ell|^2 \right. \\ &\left. - \frac{h}{N}\sum_\ell \Gamma_\ell \varphi_\ell \left(\varphi_1\varphi_{-1-\ell} + \varphi_{-1}\varphi_{1-\ell}\right)\right\rangle. \end{aligned} \tag{39}$$

In order to proceed, it is necessary to invoke a relationship between $|\boldsymbol{m}|^2$ and the higher-order Fourier modes. Motivated by symmetry considerations, we impose the closure $\varphi_\ell\varphi_{-j}\varphi_{j-\ell} = |\varphi_1|^2\varphi_0$ for all $l \in \mathbb{Z}$ and $j \in \{-1,0,1\}$, which is exact in both the $|\boldsymbol{m}|^2 \to 0$ and $|\boldsymbol{m}|^2 \to 1$ limits. In this regime, using the fact that $\sum_\ell \Gamma_\ell = 3$, Eq. (39) then simplifies to

$$\begin{aligned}\frac{d}{dt}\langle|\boldsymbol{m}|^2\rangle = \Big\langle &-2a|\boldsymbol{m}|^2 + 2h|\boldsymbol{m}|^2\left(1-|\boldsymbol{m}|^2\right) \\ &+ \frac{2}{N}\left[a + (c+h)\left(1-|\boldsymbol{m}|^2\right)\right]\Big\rangle. \end{aligned} \tag{40}$$

As a result, using the ansatz (30), the SDE for $\boldsymbol{m}$ becomes

$$\begin{aligned}\frac{d\boldsymbol{m}}{dt} &= -a\boldsymbol{m} + h\boldsymbol{m}\left(1-|\boldsymbol{m}|^2\right) \\ &+ \sqrt{\frac{a+(c+h)\left(1-|\boldsymbol{m}|^2\right)}{N}}\,1\cdot\boldsymbol{\eta}(t), \end{aligned} \tag{41}$$

and the stationary distribution for the norm is

$$P(|\boldsymbol{m}|) \propto |\boldsymbol{m}|\,\left[a+(c+h)\left(1-|\boldsymbol{m}|^2\right)\right]^{\frac{Na(c+2h)}{(c+h)^2}-1} e^{\frac{|\boldsymbol{m}|^2 hN}{c+h}}. \tag{42}$$

III. MEAN-FIELD STOCHASTIC SIMULATIONS

A. Numerical solutions of the extracted SDE

After extracting Eq. (3) from the data by fitting jump-moments, we used the Milstein-method implemented by the commercial software Mathematica [41] to numerically generate solutions in order to ensure that it gives rise to the correct governing statistics (see Extended Data Figure 2).

As a technical aside, we remark that these PDFs all suffer from the same deficiency. They are defined on an open domain ($\mathbb{R}^2$) rather than the unit disk, which is the case for the experimental data. The reason for this is that there is no systematic way to extract the necessary 'reflecting-SDE' from either the data, or indeed a given Fokker-Planck equation. To our knowledge, this issue arises in all such studies, including exactly solvable toy models, such as [13, 17], which we discuss in Supplementary Section IV.

B. Gillespie simulations

The data presented in Fig. 4 was generated via continuous-time stochastic Gillespie [42, 43] simulations of the relevant microscopic models (both pairwise and ternary). For brevity, only the first jump moments and the steady-state PDFs are shown. For completeness, the non-zero coefficients of the second jump-moments are included in Extended Data Figure 3.

C. Higher-order copying interactions

In Section V, we describe an explicit example of a ternary copying interaction, which can be shown to poorly represent the data when the parameters take certain values. More systematically, we considered a range of such individual-based n-body copying models, and used extensive computer simulations to optimise their parameters against the data. Specifically, we considered mean-field n-body interactions that were of the form

$$\theta_{i_1} + \theta_{i_2\neq i_1} + \ldots + \theta_{\substack{i_n\neq i_1\\ \neq i_2\\ \vdots\\ \neq i_{n-1}}} \xrightarrow{r_n} \begin{cases} 2\theta_{j_1} + \theta_{j_2} + \ldots + \theta_{j_{n-1}} \\ \theta_{j_1} + 2\theta_{j_2} + \ldots + \theta_{j_{n-1}} \\ \quad\vdots \qquad\quad \vdots \\ \theta_{j_1} + \theta_{j_2} + \ldots + 2\theta_{j_{n-1}} \end{cases}, \tag{43}$$

where

$$\{j_1, j_2, \ldots, j_{n-1}\} = \underset{\{X\subset\{i_1,i_2,\ldots,i_n\}:|X|=n-1\}}{\arg\max} \left|\sum_{k\in X}\begin{pmatrix}\cos\theta_k \\ \sin\theta_k\end{pmatrix}\right|. \tag{44}$$

This is a straightforward extension of the ternary interaction described in Section V. With a specific rate r_n, n individuals are picked at random and their directions are compared in order to find the $(n-1)$ individuals that are most aligned. The remaining individual then turns to copy the direction

of any of the others with equal probability. In this context, we used the Gillespie algorithm [42, 43] to simulate individuals subject to both spontaneous changes in direction [*cf.* Eq. (5)] and n-body copying interactions of the above form [Eqs. (43) and (44)]. We characterised each model by the integer n, such that copying interactions were included up to n-body. That is, if $n = 4$, the model contained 2-, 3-, and 4-body interactions *etc.* (Self-interactions have no meaning here). As a result, each simulation required n specific rates, $r_1, \ldots, r_n$ (with r_1 corresponding to spontaneous direction change s, r_2 corresponds to pairwise copying rate c, and r_3 to ternary interaction rate h). Employing a Genetic Algorithm (GA) [44], Gillespie runs were then used to generate steady-state PDFs $P_{N,r_1,\ldots,r_p,\varepsilon}(|\boldsymbol{m}|)$, which were optimised against the data, for a given N, by minimising the Kullback-Leibler (KL) divergence $D_{KL}\left[P_{N,r_1,\ldots,r_p,\varepsilon}(|\boldsymbol{m}|)\,||\,P_N(|\boldsymbol{M}|)\right]$. Once the optimal rates had been found, we re-computed the KL divergence many times in order to obtain statistics that further account for the inherent variation associated with different Gillespie runs (using the same parameters).

The results are shown in Extended Data Table 1, where it is clear that, in each instance, the GA returns models whose fit with the steady-state statistics of the data is very good and the D_{KL} values (taken along with its respective $\sigma^2\{D_{KL}\}$) are comparable across the different models for a given N. From the optimised rates corresponding to each of the model, it is clear that all n- body interactions above pairwise (*i.e.*, $n > 2$) are negligible. That is, the data (and its underlying noise-induced character) can be viewed as strong evidence for underlying interactions that are pairwise-dominant.

As a technical aside, we note that, in practice, the KL divergence differs slightly with each Gillespie 'run'. However, repeated runs using the GA-optimised rates indicate that the small differences in KL divergence that appear in Extended Data Table 1 for different models— *i.e.,* different n— are well within this expected statistical variation.

Further, we note that the pairwise copying rate ($r_2 \approx 8$ in Extended Data Table 1) is comparable but almost double the value of the copying rate we reported in the main text ($c = \beta \approx 4$). This is because the above optimum rates for each of the higher-order interaction model was obtained by fitting the *1D histogram of the group polarisation (scalar* $|\boldsymbol{M}|$*)* of the data to that of simulations. In contrast, the pairwise copying rate in the main text was found by the best-fit function of *jump-moments of the group polarisation (vector* $\boldsymbol{M}$*)* of the data. We may modify the optimisation procedure if the objective function is defined accounting for jump moments. However, this is computationally demanding because of a very large time series of the data that is required to compute the jump moments. Despite the difference in the methods used, it is striking that the estimated rates are comparable. Importantly, these estimated parameters for each of the above models suggest that the dominant interaction always corresponds to pairwise copying.

D. Higher-order Vicsek-like interactions

Given its prevalence in the collective motion literature, we wanted to explicitly compare our results with any Vicsek-like behaviour, where alignment results from individuals averaging the directions of a number of neighbours. For comparison with our existing results, we consider an individual-based analogue of the Vicsek model that is mean-field— *i.e.*, it does not describe spatially distributed collectives, and all individuals are technically 'neighbours'. Here, individuals can perform one of two actions. Specifically, they can change their direction at random [*cf.* Eq. (5)], or they choose $n-1 \leq N$ other individuals, and turn to move towards the average direction of those individuals . That is

$$\theta_{i_1} + \theta_{i_2 \neq i_1} + \ldots + \theta_{\substack{i_n \neq i_1 \\ \neq i_2 \\ \vdots \\ \neq i_n}} \xrightarrow{r_n} \frac{1}{n-1}\Big(\sum_{j=2}^{n} \theta_{i_j}\Big) + \theta_{i_2} + \ldots + \theta_{i_n}. \tag{45}$$

This has the benefit that, for $n = 2$, we recover the pairwise copying interaction used throughout our study, and yet higher order terms follow the canonical direction-averaging protocol of the Vicsek model in the limit of no error.

Once again using a GA to scan the relevant parameter space, repeated Gillespie simulations indicate that the KL-divergence between the PDF extracted from the data and that generated from simulations is minimised by pairwise interactions— *i.e.*, $n = 2$— and that any kind of higher-order direction averaging ($n \geq 3$) results in considerable mismatch (large values of D_{KL}) that cannot be attributed to the inherent fluctuations associated with Gillespie simulations (see Extended Data Table 2).

[32] Jhawar, J., Guttal, V. Noise-induced effects in collective dynamics and inferring local interactions from data. Preprint at https://arxiv.org/abs/1911.09376 (2019).

[33] Lukeman, R., Li, Y. X., and Edelstein-Keshet, L. Inferring individual rules from collective behavior. *Proc. Natl. Acad. Sci.*, **107,** 12576–12580 (2010).

[34] Katz, Y., Tunstrøm, K., Ioannou, C. C., Huepe, C., and Couzin, I., D. Inferring the structure and dynamics of interactions in schooling fish. *Proc. Natl. Acad. Sci.*, **108,** 18720–18725 (2011).

[35] Puckett, J.G., Ni, R. and Ouellette, N.T. Time-frequency analysis reveals pairwise interactions in insect swarms. *Phys. Rev. Lett.*, **114,** 258103 (2015).

[36] Calovi, D. S. et al. Disentangling and modeling interactions in fish with burst-and-coast swimming reveal distinct alignment and attraction behaviors. *PLoS Comp. Biol.*, **14,** e1005933 (2018).

[37] Gardiner, C. *Handbook of Stochastic Methods*, **3**. (Springer, Berlin, 2003).

[38] Kirman, A. Ants, rationality, and recruitment. *Q. J. Econ.*, **108,** 137–156 (1993).

[39] Alfarano, S., and Lux, T. A noise trader model as a generator of apparent financial power laws and long memory. *Macroecon. Dyn.*, **11,** 80–101 (2007).

[40] Minors, K., Rogers, T., and Yates, C. A. Noise-driven bias in the non-local voter model. *Europhys. Lett.*, **122,** 10004 (2018).
[41] Wolfram Research Inc., Mathematica Version 10.0, 2014.
[42] Gillespie, D. T. A general method for numerically simulating the stochastic time evolution of coupled chemical reactions. *J. Comput. Phys.*, **22,** 403–434 (1976).
[43] Gillespie, D. T. Exact stochastic simulation of coupled chemical reactions. *J. Phys. Chem.*, **81,** 2340–2361 (1977).
[44] Goldberg, D. E. *Genetic Algorithms in Search, Optimization & Machine Learning.* (Addison-Wesley, Boston MA, 1989).

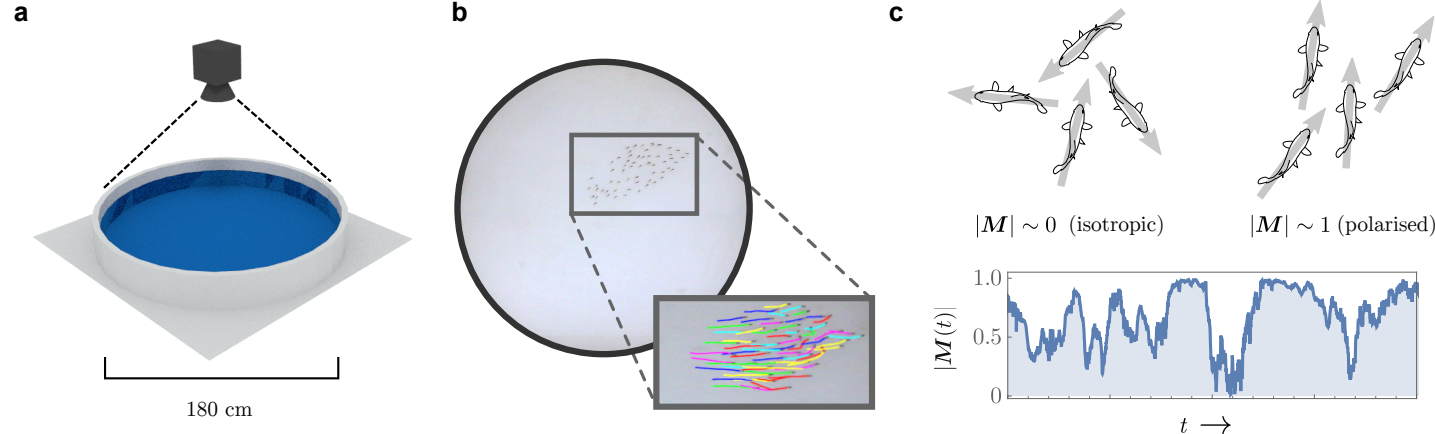
a
180 cm
b
c
$|\boldsymbol{M}| \sim 0$ (isotropic)
$|\boldsymbol{M}| \sim 1$ (polarised)
1.0
0.5
0
$|\boldsymbol{M}(t)|$
$t \longrightarrow$

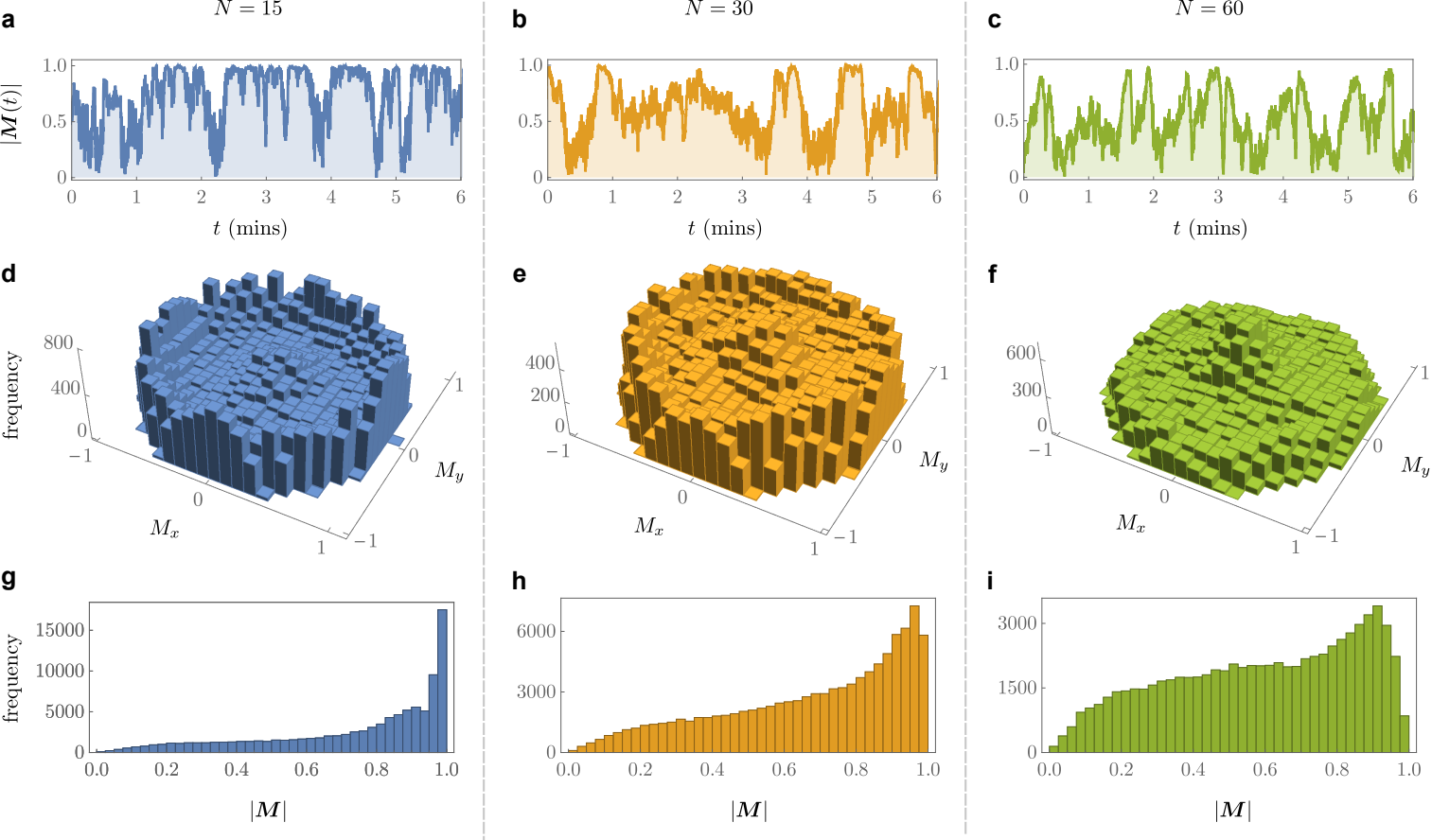
a
$N = 15$
$|M(t)|$
1.0
0.5
0
0 1 2 3 4 5 6
t (mins)
b
$N = 30$
1.0
0.5
0
0 1 2 3 4 5 6
t (mins)
c
$N = 60$
1.0
0.5
0
0 1 2 3 4 5 6
t (mins)
d
frequency
800
400
0
−1 0 1
M_x
1 0 −1
M_y
e
400
200
0
−1 0 1
M_x
1 0 −1
M_y
f
600
300
0
−1 0 1
M_x
1 0 −1
M_y
g
frequency
15000
10000
5000
0
0.0 0.2 0.4 0.6 0.8 1.0
$|M|$
h
6000
3000
0
0.0 0.2 0.4 0.6 0.8 1.0
$|M|$
i
3000
1500
0
0.0 0.2 0.4 0.6 0.8 1.0
$|M|$

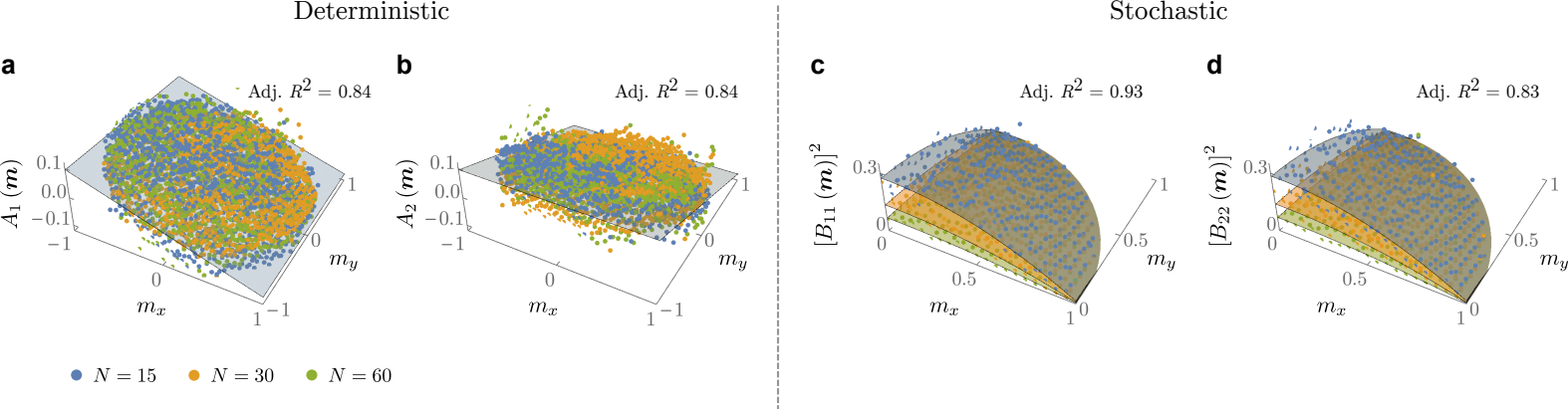
Deterministic
Stochastic
a
b
c
d
Adj. $R^2 = 0.84$
Adj. $R^2 = 0.84$
Adj. $R^2 = 0.93$
Adj. $R^2 = 0.83$
$A_1(\boldsymbol{m})$
$A_2(\boldsymbol{m})$
$[B_{11}(\boldsymbol{m})]^2$
$[B_{22}(\boldsymbol{m})]^2$
m_x
m_y
$N = 15$
$N = 30$
$N = 60$

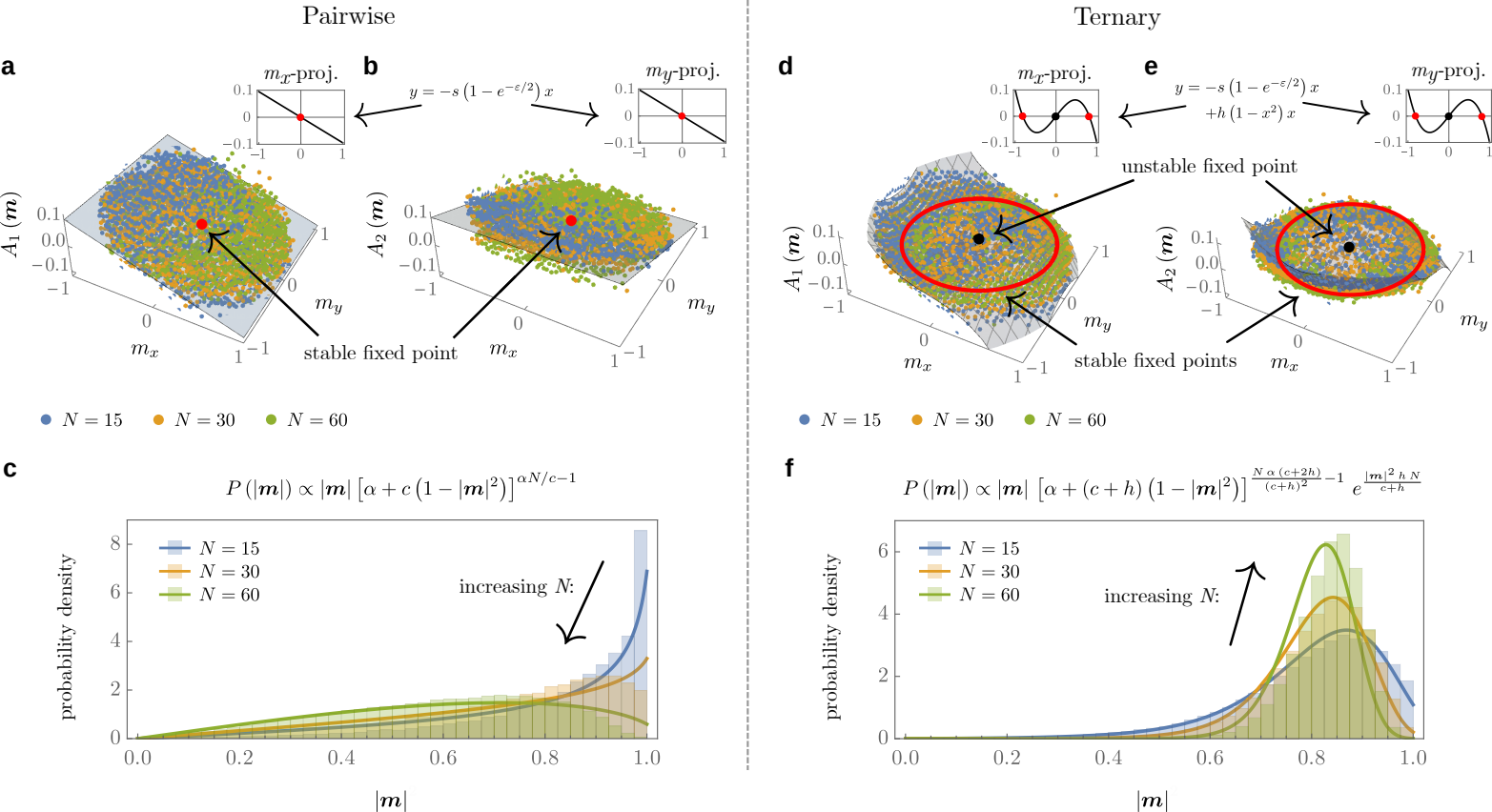
Pairwise
Ternary
a
b
d
e
c
f
m_x-proj.
m_y-proj.
$y = -s\,(1 - e^{-\varepsilon/2})\,x$
$y = -s\,(1 - e^{-\varepsilon/2})\,x + h\,(1 - x^2)\,x$
$A_1(\boldsymbol{m})$
$A_2(\boldsymbol{m})$
m_x
m_y
stable fixed point
unstable fixed point
stable fixed points
$N = 15$
$N = 30$
$N = 60$
$P(|\boldsymbol{m}|) \propto |\boldsymbol{m}|\,\left[\alpha + c\,(1 - |\boldsymbol{m}|^2)\right]^{\alpha N/c - 1}$
$P(|\boldsymbol{m}|) \propto |\boldsymbol{m}|\,\left[\alpha + (c+h)\,(1 - |\boldsymbol{m}|^2)\right]^{\frac{N\,\alpha\,(c+2h)}{(c+h)^2} - 1}\, e^{\frac{|\boldsymbol{m}|^2\,h\,N}{c+h}}$
increasing N:
probability density
$|\boldsymbol{m}|$

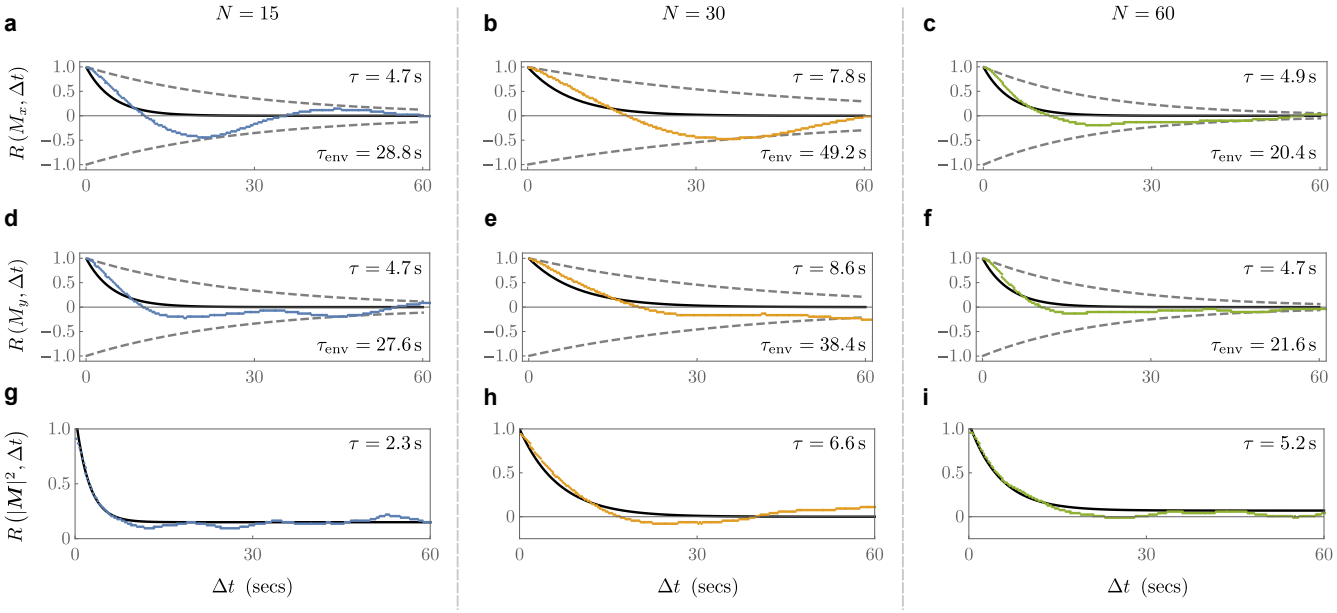

Extended Data Figure 1. **Autocorrelation of group polarisation**. Blue, yellow and green solid lines represent the data for $N = 15$, 30, and 60, respectively. Two characteristic time-scales are apparent; τ, which encapsulates the rate of initial decay of correlations to zero (solid black lines) and τ_{env}, which is rate of decay of the envelope of quasi-periodic correlations (dotted grey lines).

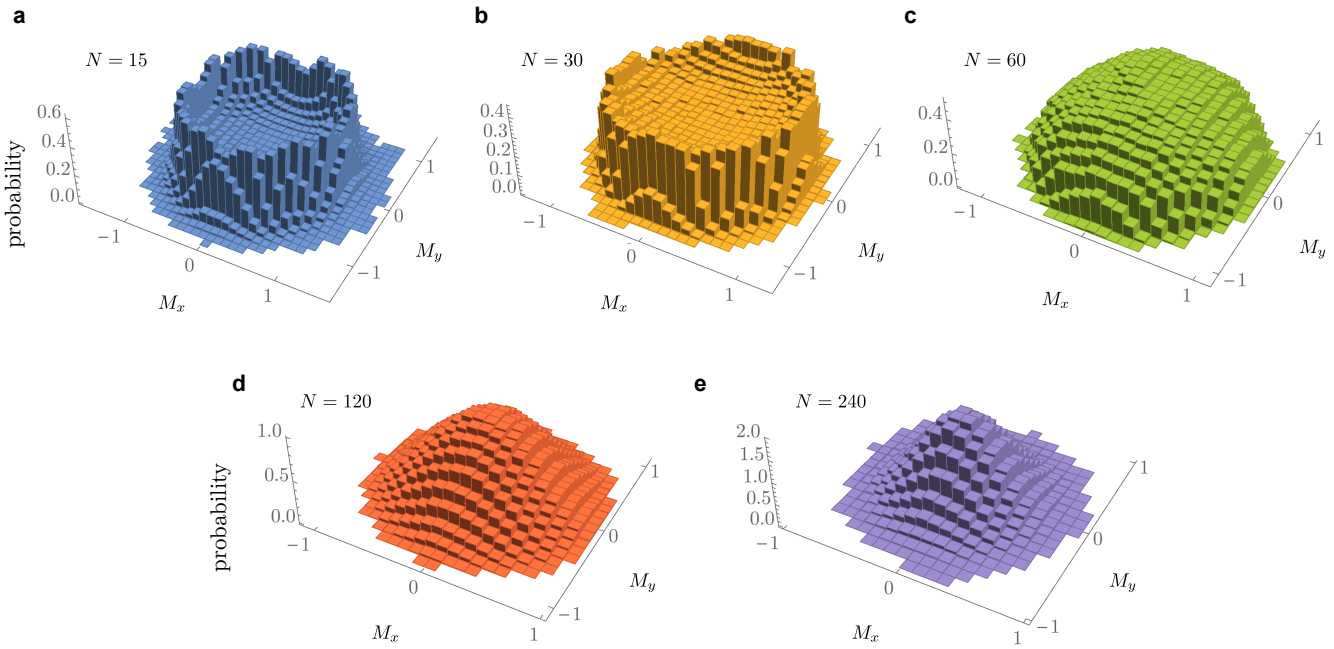

Extended Data Figure 2. **Numerical check of the extracted SDE**. Milstein-method simulations of the SDE that was extracted from the data [Eq. (3) of the main manuscript]. The results are qualitatively in-line with experimental observations.

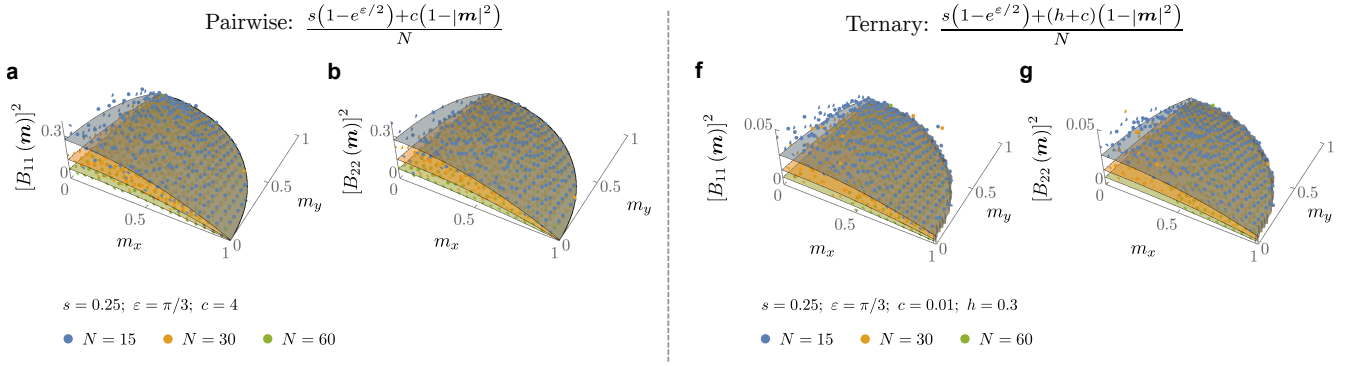

Extended Data Figure 3. **Second jump-moments: pairwise vs. ternary**. In agreement with theoretically derived expressions, the simulation-generated diagonal (non-zero) second jump-moments take a similar form for both pairwise and ternary models. Data points are generated by Gillespie simulation (using the stated parameter values), whilst both surfaces and the analytical expressions to which they correspond are taken from theory (Methods Sections II A & B).

Extended Data Table 1. **Optimisation of higher-order copying interaction models**. Using a Genetic Algorithm in the context of repeated Gillespie simulations (Methods Section III C), we optimise a given model's specific rates against the experimental data. The results – specifically, large values of r_2 and negligible values of r_i where $i > 2$ – imply that pairwise copying is the dominant mode of interaction and that higher order interactions are likely negligible.

N	p	Rates	$\overline{D_{KL}\left[P_{N,r_1,...,r_p,\varepsilon}\left(\lvert\boldsymbol{m}\rvert\right)\,\lvert\rvert\,P_N\left(\lvert\boldsymbol{M}\rvert\right)\right]}$	$\sigma^2\left\{D_{KL}\left[P_{N,r_1,...,r_p,\varepsilon}\left(\lvert\boldsymbol{m}\rvert\right)\,\lvert\rvert\,P_N\left(\lvert\boldsymbol{M}\rvert\right)\right]\right\}$
15	2	$r_1 = 0.48$ $r_2 = 7.99$	0.0504	0.0012
	3	$r_1 = 0.47$ $r_2 = 7.40$ $r_3 = 0.01$	0.0503	0.0012
	4	$r_1 = 0.48$ $r_2 = 7.69$ $r_3 = 0.00$ $r_4 = 0.00$	0.0498	0.0013
	5	$r_1 = 0.48$ $r_2 = 7.19$ $r_3 = 0.00$ $r_4 = 0.00$ $r_5 = 0.00$	0.0500	0.0012
30	2	$r_1 = 0.32$ $r_2 = 8.41$	0.0314	0.0018
	3	$r_1 = 0.32$ $r_2 = 8.59$ $r_3 = 0.00$	0.0312	0.0016
	4	$r_1 = 0.35$ $r_2 = 8.46$ $r_3 = 0.04$ $r_4 = 0.02$	0.0322	0.0016
	5	$r_1 = 0.33$ $r_2 = 8.41$ $r_3 = 0.01$ $r_4 = 0.00$ $r_5 = 0.02$	0.0320	0.0017
60	2	$r_1 = 0.23$ $r_2 = 8.49$	0.0460	0.0042
	3	$r_1 = 0.24$ $r_2 = 8.41$ $r_3 = 0.01$	0.0478	0.0044
	4	$r_1 = 0.24$ $r_2 = 8.65$ $r_3 = 0.00$ $r_4 = 0.01$	0.0475	0.0039
	5	$r_1 = 0.25$ $r_2 = 8.72$ $r_3 = 0.02$ $r_4 = 0.01$ $r_5 = 0.00$	0.0478	0.0047

Extended Data Table 2. **Optimisation of higher-order Vicsek-like interaction models.** Using a Genetic Algorithm in the context of repeated Gillespie simulations for higher-order Vicsek-like interaction models (Methods section III D), we optimise a given model's specific rates against the experimental data. The results confirm that direction-averaging (represented by r_i where $i > 2$) is not represented by the data; this can be inferred from the values of the D_{KL} corresponding to the optimized rates of interaction.

N	n	Rates	$\overline{D_{KL}\left[P_{N,\,r_1,\,r_n,\,\varepsilon}\left(\lvert\boldsymbol{m}\rvert\right)\,\lvert\rvert\,P_N\left(\lvert\boldsymbol{M}\rvert\right)\right]}$	$\sigma^2\left\{D_{KL}\left[P_{N,\,r_1,\,r_n,\,\varepsilon}\left(\lvert\boldsymbol{m}\rvert\right)\,\lvert\rvert\,P_N\left(\lvert\boldsymbol{M}\rvert\right)\right]\right\}$
15	2	$r_1 = 0.48$	0.0504	0.0014
		$r_2 = 7.99$		
	3	$r_1 = 0.85$	0.2250	0.0022
		$r_3 = 7.16$		
	4	$r_1 = 1.07$	0.3228	0.0024
		$r_4 = 6.28$		
	5	$r_1 = 1.22$	0.3821	0.0018
		$r_5 = 6.87$		
30	2	$r_1 = 0.32$	0.0314	0.0018
		$r_2 = 8.41$		
	3	$r_1 = 1.45$	0.4062	0.0047
		$r_3 = 9.20$		
	4	$r_1 = 1.95$	0.5967	0.0042
		$r_4 = 7.21$		
	5	$r_1 = 2.47$	0.7179	0.0045
		$r_5 = 8.44$		
60	2	$r_1 = 0.23$	0.0460	0.0042
		$r_2 = 8.49$		
	3	$r_1 = 2.31$	0.5710	0.0068
		$r_3 = 8.36$		
	4	$r_1 = 3.94$	0.7408	0.0065
		$r_4 = 8.71$		
	5	$r_1 = 5.58$	0.8545	0.0065
		$r_5 = 9.29$		